PERSPECTIVE

Check for updates

Prospects and challenges in designing photocatalytic particle suspension reactors for solar fuel processing†

Swarnava Nandy, ‡ Sangram Ashok Savant ‡ and Sophia Haussener *

Photocatalytic approaches for the production of solar hydrogen or hydrocarbons are interesting as they provide a sustainable alternative to fossil fuels. Research has been focused on water splitting and on the synthesis of photocatalyst materials and compounds, and their characterization. The material-related challenges include the synthesis and design of photocatalysts that can absorb visible light at a high quantum efficiency, cocatalysts that are selective and can accelerate the reduction and/or oxidation reactions, and protection layers that facilitate migration of the minority carriers to the surface-active sites while reducing charge recombination and photo-corrosion. Less attention has been paid to the conceptual design of reactors, and how design and coupled transport can affect the material choice and requirements. This perspective discusses the various possible conceptual designs for particle suspension reactors and the related implications on the material requirements to achieve high energy conversion efficiencies. We establish a link between the thermodynamic limits, materials requirements, and conceptual reactor designs, quantify changes in material requirements when more realistic operation and losses are considered, and compare the theory-derived guidelines with the ongoing materials research activity.

1. Introduction

Photocatalytic solar fuel production is a promising way to provide clean and storable fuels using only sunlight and abundant reactants such as water or CO_2.[1–3] Photocatalytic approaches use catalytically active semiconductor particles (suspended in liquid electrolytes) that absorb photons with sufficient energy from sunlight to produce excited charge carriers (electron and hole pairs), which are separated (by diffusion and migration) and transported to catalytically active sites where they are used in reduction and oxidation reactions, respectively. Hydrogen, produced as a result of the water electrolysis reaction by sunlight, is a clean and renewable energy carrier, used extensively in fuel cells and hydrogen combustion engines. Hydrogen can be stored liquefied, compressed, as metal-hydride, or in the form of hydrocarbons, ammonia and alcohol. Combustion of hydrogen only produces water, a by-product which does not cause any pollution. Consequently, if hydrogen can be produced by water splitting and with renewable resources, it becomes an extremely attractive energy carrier. The concurrently occurring water oxidation reaction produces oxygen, a component enabling life.

In 1980, overall water splitting into stoichiometric hydrogen and oxygen was reported on NiO–SrTiO$_3$ photocatalyst particles suspended in water, considered as one of the earliest example of water splitting using a particulate approach.[4] Research has since focused on developing visible-light driven photocatalysts in order to realize efficient overall water splitting by sunlight. Similarly, carbon dioxide can be directly converted to various hydrocarbons by photocatalytic reactions.[5,6] One main challenge for photocatalytic approaches remains the discovery, synthesis and design of photocatalysts that can use a larger portion of the solar spectrum (mostly the longer wavelength photons) and that can stably evolve hydrogen and oxygen gases for several days, as well as the development of reactor concepts that allow for the practical implementation and scaling of photocatalyst suspension-based hydrogen processing plants.[7] More recently, implementation and theoretical investigations of complete photocatalyst particle suspension reactors have indicated that not only the individual materials need to be optimized, but their interactions need to be understood and optimized concurrently.[8] Additionally, the best choice of material combinations will depend on the reactor concepts and *vice versa*.

In photocatalysis, apparent quantum yield (AQY) and, to a lesser extent, solar-to-hydrogen (STH) conversion efficiencies have been used to compare performance of the systems.[3,9] AQY

Laboratory of Renewable Energy Science and Engineering, Institute of Mechanical Engineering, EPFL, Station 9, 1015 Lausanne, Switzerland. E-mail: sophia.haussener@epfl.ch; Tel: +41 21 69 33878

quantifies the photons utilized for water splitting compared to the total number of photons provided to the system. STH is defined as the chemical energy content of the produced fuel compared to the solar energy incident to the system $\left(STH = \dfrac{\dot{m}''_{H_2} \Delta G}{\dot{P}_{solar}} = \dfrac{i_{H_2} \Delta E}{\dot{P}_{solar}} \right)$. Some metal oxides are known to show excellent AQY but most of them are active only under sunlight's UV spectrum (accounting for only ~10% of the solar irradiation energy).[10,11] Photocatalysts with much smaller bandgaps are needed to utilize a significant portion of the solar spectrum.[12,13] However, not only the band gap energy of the photocatalyst needs to be large enough to provide sufficient energy for water splitting reaction while being small enough to absorb a large fraction of the visible light, but also the position of the valence and conduction band of the photocatalyst have to straddle the oxygen evolution and hydrogen evolution reaction potential, therefore further limiting the choice of materials.[3] A complementing approach on the quest to increase the efficiency consists of developing tandem systems, *i.e.* approaches which use two step photoexcitation, also called Z-scheme approaches.[14,15] This approach allows for higher efficiencies and provides more flexibility as two materials are combined and a wider variety of materials can be exploited for hydrogen and oxygen evolution reactions.[16] Several combinations of metal oxides and non-oxide photocatalysts for H_2 and O_2 gas evolution have been studied to realize Z-scheme overall water splitting.[17,18] But all the reported systems suffer from low energy conversion efficiency and lack in long-term stability. Z-scheme approaches require the transport of electron from the oxygen evolution photocatalyst (OEP) to hydrogen evolution photocatalyst (HEP), for example by utilizing a liquid redox mediator (Fig. 1b) or a solid-state mediator. The selection of photocatalysts with appropriate redox mediators still remains an issue for efficient overall water splitting, given activity, selectivity, reversibility and stability issues of HEP and OEP in the corresponding mediator solutions.

Many of the practical demonstrations and implementations of Z-scheme photocatalyst suspensions into scalable reactors are not suitable for product separation as they lead to the cogeneration of hydrogen and oxygen gasses at the near same location. Implementation of photocatalysts into a practical device that generates separated and clean streams of hydrogen and oxygen at high efficiency, low cost, sustainably, and stably is not yet sufficiently addressed. There are review articles that address the materials engineering and roles of various cocatalysts to improve charge transfer efficiency in semiconductor particulate to obtain higher rates of solar energy conversion,[17–19] but much less attention has been paid to designing and comparing conceptual particulate suspension reactors. It is unclear how the conceptual design of such a reactor will affect the overall performance, what are the limiting efficiencies and how they depend on the design, what are the general material requirements and how – in turn – the design will affect the best choice of materials.[8] Furthermore, the coupled heat, mass, and charge transport in such reactors[20] will affect the local environment at which the photocatalyst and co-catalyst operate, potentially influencing activity, selectivity and stability while also leading to heterogeneous performance in the reactor. Here, we provide a unified overview of the challenges and prospects of photocatalyst suspension water splitting approaches, considering material research-centered challenges together with the design concept-related multi-physical transport and reactor engineering challenges.

2. Principle of photocatalytic water splitting

Photocatalytic water splitting involves three fundamental steps: (i) absorption of photons with energies larger than the bandgap
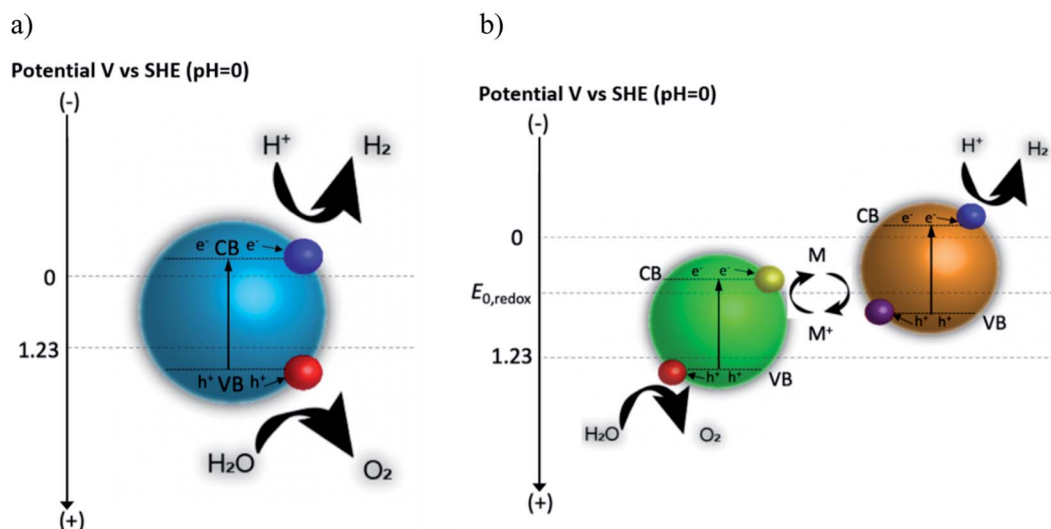

Fig. 1 Principle and energy levels of photocatalytic overall water splitting using (a) one-step photo-excitation and (b) two-step photo-excitation (Z-scheme).

energy of the semiconductor(s) to push electrons from the valence band to the conduction band while leaving behind holes, (ii) separation and transport (by diffusion and/or migration) of the excited charge carriers from the bulk to the surface, and (iii) charge transfer by chemical reaction at the surface through electrons in the conduction band, reducing proton to produce hydrogen (in acidic medium), and holes in the valence band, oxidizing water to produce oxygen (in acidic medium). The conduction band minimum (CBM) and the valence band maximum (VBM) of the photocatalyst must have potential energies more negative (with respect to SHE) and positive (with respect to SHE), respectively, than the potential of H^+/H_2 (0 V vs. SHE) and O_2/H_2O (+1.23 V vs. SHE).[3,17] In photocatalysis, this is an essential condition for a semiconductor to be able to split water as the surface is exposed to a reaction solution. This semiconductor-centric picture assumes that there is enough reactant in the solution and accessible at the surface for the chemical reaction as well as that the products are rapidly evacuated. In reality, mass, charge and heat transfer are affecting the local solution conditions at the particle surface, influencing the kinetics, degradation, and potentially also surface recombination and band bending.

If a Z-scheme is considered, then the liquid redox or solid-state mediators will additionally affect the requirements on CBM and VBM. For example, for a liquid redox mediator with a given redox potential, the CBM and VBM of the HEP have to straddle the hydrogen evolution reaction (HER) and the mediator oxidation while the CBM and VBM of the OEP have to straddle the mediator reduction and the oxygen evolution reaction (OER). Furthermore, the HEP and OEP have to be stable in the solution, and be active and selective towards the various reactions, while suppressing the reverse reactions.

Cocatalysts are frequently used to modify the surface of the photocatalyst to improve the activity and selectivity of the redox reactions. These are known to extract excited charge carriers from the bulk of the materials to their surfaces because of their greater work function, compared to the semiconductor photocatalysts.[19] Cocatalysts can accelerate water splitting reactions by reducing the overpotential of the HER and OER, or of the redox mediator oxidation and reduction reactions (in a Z-scheme with liquid mediator). Cocatalysts facilitate the migration of electrons and holes from the conduction and valence bands of the photoabsorber to the active sites of the catalyst for the reduction and oxidation reactions, respectively. Nobel metals such as Pt, Rh, Ru are widely used as reduction cocatalysts for H_2 evolution reaction, whereas metal oxides and sulfides such as IrO_2, $NiFeO_x$, RuO_2, CoO_x, PdS, NiS, Ag_2S are known to act as oxidation cocatalyst to promote oxygen evolution reaction.[19,21] Not all of these cocatalysts are equally stable for the complete pH range. For example, from photoelectrochemistry it is known that OER catalysts are typically more stable in alkaline conditions while HER catalysts have demonstrated stability in a larger pH range.[22,23]

A large fraction of charge carriers produced as a result of the photoexcitation do not participate in the oxidation and reduction reactions due to inefficient semiconductor charge transfer from the bulk to surface active sites (bulk and surface recombination) and due to activity and selectivity issues of the reactions. Charge recombination and competing reactions are responsible for lowering the water splitting activity and are major reasons why none of the reported lab-scale demonstrations have achieved STH efficiencies above 1–2%. For laboratory demonstrations, photocatalytic water splitting has often been performed in the presence of sacrificial reagents or redox mediators, generally known as half reaction water splitting for HER or OER. It is rarer to find overall water splitting demonstrations.

2.1 Half reaction water splitting for hydrogen or oxygen evolution

Test reactions are often performed for newly developed photocatalytic materials before considering them for overall water splitting.[24] These reactions are usually conducted in the presence of sacrificial electron donors or acceptors. For the HER, excited e^- in the conduction band travel to surface active sites to reduce H^+ to hydrogen (in acidic medium), whereas holes in the valence band are consumed by the sacrificial electron donors (e.g. CH_3OH, Na_2S). Thus, no oxygen evolution is observed. For OER, excited h^+ in the valence band travel to surface active sites for the oxidation reaction to produce O_2 and e^- in the conduction band are captured by the sacrificial electron acceptors (e.g. $AgNO_3$). Consequently, no hydrogen evolution is observed. Instead of sacrificial electron donor or acceptor, water splitting half reactions can (or should) also be performed in the presence of reversible electron donors (for example Fe^{2+} or I^-) or acceptors (for example Fe^{3+} or IO_3^-) for HER and OER, respectively. These experiments provide a more relevant investigation of newly developed materials for the half reactions, given that these reversible electron donors or acceptors can be used as liquid redox mediator (discussed in Section 2.2) and therefore enable overall water splitting with spatially separated hydrogen and oxygen production. A newly developed material can be investigated with sacrificial electron donors and acceptors (or for redox mediator oxidation or reduction), where the measured H_2 and/or O_2 gas evolution rates indicate whether the material can sustain overall water splitting or only one of the half reactions (i.e. act as HEP or OEP).

2.2 Overall water splitting for H_2 and O_2 gas evolution

Overall water splitting is performed using either one photocatalyst (simultaneously promoting OER and HER) in a one-step photoexcitation or using two photocatalysts (one promoting OER and mediator reduction, and one promoting HER and mediator oxidation) in a two-step photoexcitation, widely known as Z-scheme (Fig. 1b).[3,18] Only few materials meet the criteria of band straddling for overall water splitting in a one-step photoexcitation to evolve hydrogen and oxygen gases while absorbing a large fraction of the solar spectrum. Consequently, only very few examples have been reported, including GaN:ZnO solid solution,[25] β-Ge_3N_4,[26] Al-doped $SrTiO_3$ ($SrTiO_3$:-Al)[11] and Ta_3N_5.[27] However, implementing these materials in a practical photocatalytic reactor will lead to the co-evolution of hydrogen and oxygen in close vicinity (within a distance of
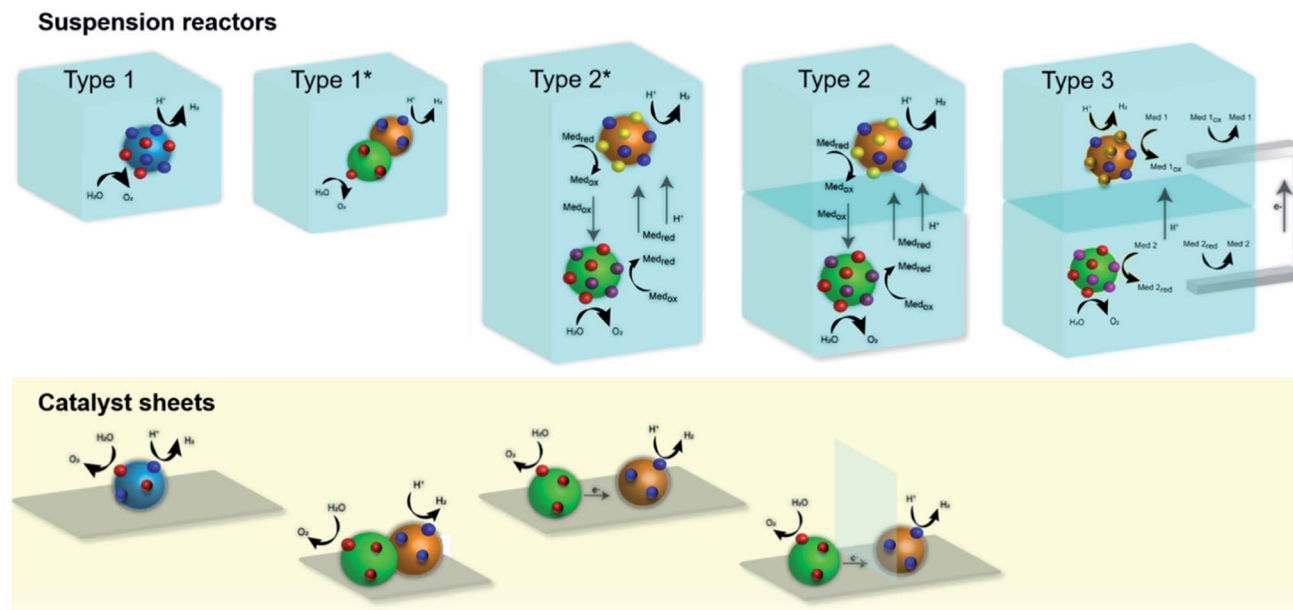
Suspension reactors

Catalyst sheets

Fig. 2 Schematic designs of different conceptual powder suspension (top line) and catalyst sheet reactors (bottom line). The catalyst sheets consist of the immobilized-photocatalyst in analog configuration to the suspension reactor. The color scheme of the cocatalysts indicates the selective photocatalysts for HER (blue), OER (red), mediator reduction (dark and light violet) and mediator oxidation (light and dark yellow). Types 2 and 3 include a membrane, and type 3 includes a wire.

a particle diameter), requiring a dedicated separation process downstream, posing safety issues, and reducing the product yield. Z-scheme approaches have the potential to allow for spatially separated evolution of hydrogen and oxygen as well as providing a larger choice for the materials selection (Fig. 1b). HEP and OEP can be chosen based on narrow bandgap materials to absorb visible light and half reaction gas evolution activity in the presence of reversible mediator species with sufficient driving force. Z-scheme overall water splitting is kinetically more challenging compared to one-step overall water splitting as it involves more charge transfer steps but is thermodynamically more efficient as multiple photoabsorbers with different band gaps can be easily used. An electron shuttle in the form of a reversible solution based redox mediator (for *e.g.* Fe^{3+}/Fe^{2+} or IO_3^-/I^- *etc.*) or solid-state mediator (*e.g.* gold, carbon) is needed to facilitate e^- transfer from OEP to HEP.[17,18] Photocatalyst sheets (Fig. 2) have been fabricated to construct a practical Z-scheme approach where HEP and OEP particles are immobilized on a glass plate with an underlying conductive (gold or carbon) layer.[17] The photocatalytic activity of these sheets is almost independent of the pH of the solution, suggesting that the e^- transfer takes place through the conductive solid layer rather than through the solution between the particles. Z-Scheme designs based on a photocatalyst sheet achieved significantly higher efficiencies compared to its analogue in the form of a powder suspension with a soluble redox mediator. However, it is not straight forward to separately collect clean hydrogen and oxygen streams from a photocatalysts sheet. More practical (in the sense of product separation and safety) is the construction of a Z-scheme arrangement that spatially separates the H_2 or O_2 evolution, either through the immobilization of

OEP and HEP on separate sheets and their connection through an external wire acting as solid mediator (a configuration that resembles a traditional photoelectrochemical approach) or to use particle suspension approaches where the OEP and HEP particle suspensions are spatially separated by a semipermeable membrane and a liquid redox mediator is shuttling the charge between them.

An ideal redox couple is expected to have the following properties: (i) high reversibility under the relevant reaction conditions, (ii) low parasitic absorption of UV and visible light, and (iii) a suitable redox potential (between the water reduction and oxidation potentials). It is challenging to construct an efficient Z-scheme system even if all these redox mediator requirements are satisfied due to the occurrence of back reactions on both, HEP and OEP. High concentrations of the oxidized form of the mediator suppresses or compete with the H_2 evolution at the HEP. Similarly, at the OEP, high concentrations of the reduced form of the mediator reduce the O_2 evolution. Therefore, the reaction conditions and the coupled transport have to be carefully controlled so that appropriate concentrations of redox mediator in the HEP and OEP suspensions are achieved that facilitate H_2 and O_2 evolution, respectively, in the forward direction. Also, the development of dedicated cocatalysts and coatings might help in overcoming some of these reversibility issues.

Frequently used water-soluble redox mediators are $Fe^{3+/2+}$, $[Fe(CN)_6]^{3-/4-}$, IO_3^-/I^- and I_3^-/I^-. Most of these redox mediators don't work in a wide range of pH. For instance, $Fe^{3+/2+}$, $[Fe(CN)_6]^{3-/4-}$ and I_3^-/I^- can work effectively only at pH < 2.5, 6–7 and 4.5, respectively. The selective pH working range for the mediators also limits the choice of the photocatalysts to be

Table 1 List of HEPs, OEPs and redox mediators used for visible-light-driven Z-scheme overall water splitting[35,42–64]

HEP	OEP	Mediator	pH	Light source, wavelength (λ nm)	H_2 (μmol h^{-1})	O_2 (μmol h^{-1})	AQY% (λ nm), STH (%)	Year (ref)
Pt/STO:Cr,Ta	PtO$_x$/WO$_3$	IO$_3^-$/I$^-$	7.0	300 W Xe (>420)	1.8	0.9	0.1 (420 nm)	2001 (ref. 42)
Ru/STO:Rh	WO$_3$	Fe^{3+}/Fe^{2+}	2.4	300 W Xe (>420)	18.9	8.9	n.r.	2008 (ref. 43)
Ru/STO:Rh	BiVO$_4$	Fe^{3+}/Fe^{2+}	2.4	300 W Xe (>420)	19.2	9.7	0.3 (420 nm), 0.02 STH	2008 (ref. 43)
Ru/STO:Rh	BiVO$_4$	Fe^{3+}/Fe^{2+}	2.4	300 W Xe (>420)	122.0	61.0	4.2 (420 nm), 0.1 STH	2013 (ref. 44)
Pt/STO:Rh	WO$_3$	Fe^{2+}/Fe^{2+}	2.4	300 W Xe (>420)	7.8	4.0	0.5 (420 nm)	2004 (ref. 45)
Pt/STO:Rh	Bi$_2$MoO$_6$	Fe^{3+}/Fe^{2+}	2.4	300 W Xe (>420)	19.0	8.9	0.2 (440 nm)	2004 (ref. 45)
Pt/STO:Rh	BiVO$_4$	Fe^{3+}/Fe^{2+}	2.4	300 W Xe (>420)	15.0	7.1	0.4 (420 nm)	2004 (ref. 45)
Ru/STO:Rh	IrO$_x$/SrTiO$_3$:Rh/Sb	Fe^{3+}/Fe^{2+}	2.4	300 W Xe (>400)	3.0	1.4	n.r.	2014 (ref. 46)
Ru/STO:Rh	Bi$_4$NbO$_8$Cl	Fe^{3+}/Fe^{2+}	2.5	300 W Xe (>400)	15.0	7.0	0.9 (420 nm)	2018 (ref. 49)
Ru/STO:Rh	RuO$_2$/Bi$_4$NbO$_8$Cl	Fe^{3+}/Fe^{2+}	2.4	300 W Xe (>400)	11.3	5.8	0.7 (420 nm)	2019 (ref. 48)
Ru/STO:Rh	RuO$_2$/Bi$_4$NbO$_8$Cl	Fe^{3+}/Fe^{2+}	2.4	300 W Xe (>400)	28.0	15.3	1.3 (420 nm)	2019 (ref. 48)
Ru/STO:Rh	BiVO$_4$	[Co(bpy)$_3$]$^{3+/2+}$	3.8	300 W Xe (>420)	100.0	47.0	2.1 (420 nm), 0.06 STH	2013 (ref. 46)
Ru/STO:Rh	BiVO$_4$	[Co(phen)$_3$]$^{3+/2+}$	7.0	300 W Xe (>420)	10.0	4.8	n.r.	2013 (ref. 46)
Ru/STO:Rh	TiO$_2$:Cr,Sb	[Co(phen)$_3$]$^{3+/2+}$	7.0	300 W Xe (>420)	1.3	0.7	n.r.	2013 (ref. 46)
Pt/TaON	PtO$_x$/WO$_3$	IO$_3^-$/I$^-$	7.0	300 W Xe (>420)	24.0	12.0	0.4 (420 nm)	2005 (ref. 50)
Pt/ZrO$_2$/TaON	PtO$_x$/WO$_3$	IO$_3^-$/I$^-$	5.4	300 W Xe (420–800)	33.0	16.0	6.3 (420 nm)	2010 (ref. 51)
Pt/ZrO$_2$/TaON	RuO$_2$/TaON	IO$_3^-$/I$^-$	6.0	300 W Xe (>420)	7.0	3.0	0.1 (420 nm)	2011 (ref. 52)
Pt/ZrO$_2$/TaON	**Au/CoO$_x$/BiVO$_4$**	**[Fe(CN)$_6$]$^{3-}$/[Fe(CN)$_6$]$^{4-}$**	**6.0**	**300 W Xe (>420)**	**87.5**	**41.6**	**10.3 (420 nm), 0.5 STH**	**2018 (ref. 35)**
Pt/BaTaO$_2$N	PtO$_x$/WO$_3$	IO$_3^-$/I$^-$	Without control	300 W Xe (>420)	6.6	3.0	0.1 (420–440 nm)	2009 (ref. 53)
Pt/BaZrO$_3$–BaTaO$_2$N	PtO$_x$/WO$_3$	IO$_3^-$/I$^-$		300 W Xe (350–800)	22.4	9.3	0.0067 STH	2013 (ref. 54)
Pt/BaZrO$_3$–BaTaO$_2$N	TiO$_2$	IO$_3^-$/I$^-$		300 W Xe (350–800)	21.3	9.4	0.014 STH	2013 (ref. 54)
MgTa$_2$O$_{6-x}$N$_y$/TaON	PtO$_x$/WO$_3$	IO$_3^-$/I$^-$		300 W Xe (>420)	108.3	55.3	6.8 (420 nm)	2015 (ref. 55)
Pt/Sm$_2$Ti$_2$O$_2$S$_5$	TiO$_2$ (rutile)	IO$_3^-$/I$^-$	11.0	450 W Hg (>300)	9.0	3.2	n.r.	2014 (ref. 56)
Ru/(CuGa)$_{0.8}$Zn$_{0.4}$S$_2$	BiVO$_4$	[Co(terpy)$_3$]$^{3+/2+}$	Without control	300 W Xe (>420)	3.1	1.6	0.025 STH	2015 (ref. 57)
Pt/NiS/La$_5$Ti$_2$AgS$_5$O$_7$	PtO$_x$/WO$_3$	I$_3^-$/I$^-$	4.0	300 W Xe (>420)	11.1	5.4	0.12 (420 nm)	2019 (ref. 58)
Ru/STO:Rh	BiVO$_4$	RGO	3.5	300 W Xe (>420)	11.0	5.5	1.03 (420 nm)	2011 (ref. 59)
CrO$_x$/Ru/STO:Rh,La	BiVO$_4$:Mo	Au		300 W Xe (>420)	100.0	50.0	33 (419 nm), 1.1 STH	2016 (ref. 60)
Cr$_2$O$_3$/Ru/STO:Rh,La	**BiVO$_4$:Mo**	**Carbon**	**6.8**	**300 W Xe (>420)**	**90.0**	**45.0**	**26 (419 nm), 1.2 STH**	**2017 (ref. 61)**
RhCrO$_x$/ZrO$_2$/LaMg$_{1/3}$Ta$_{2/3}$O$_2$N	BiVO$_4$:Mo	Au		300 W Xe (>420)	1.1	0.6	0.07 (418 nm), 0.001 STH	2016 (ref. 62)
Cr$_2$O$_3$/Rh/La$_5$Ti$_2$Cu$_{0.9}$Ag$_{0.1}$S$_5$O$_7$:Ga	BiVO$_4$	Au	6.9	300 W Xe (>420)	20.0	10.0	4.9 (420 nm), 0.11 STH	2018 (ref. 63)
La$_5$Ti$_2$Cu$_{0.9}$Ag$_{0.1}$S$_5$O$_7$:Ga	CoO$_x$/LaTiO$_2$N	Au	11.0	300 W Xe (>420)	0.5	0.2	0.04 (420 nm)	2018 (ref. 64)

employed. $Fe^{3+/2+}$ or $[Fe(CN)_6]^{3-/4-}$ mediators are advantageous as the Fe^{3+} reduction involves a facile one-electron transfer and, thus, typical OEPs (e.g. WO_3, $BiVO_4$) have been successful for oxygen evolution without a cocatalyst.[28,29] But the $Fe^{3+/2+}$ couple precipitated as $Fe(OH)_3$ from Fe^{3+} at higher pH and was reversible only at pH < 2.5.[17] Therefore the corresponding photocatalysts must be stable enough under acidic condition. Only few photoabsorbers have been examined with the $Fe^{3+/2+}$ redox couple in a Z-scheme (Table 1). The Fe-based $[Fe(CN)_6]^{3-/4-}$ redox mediator can function at milder pH (6–7) compared to the commonly used $Fe^{3+/2+}$ couple. The IO_3^-/I^- redox couple works in basic condition (at pH 11) and the rapid backward reduction of IO_3^- on Pt cocatalysts loaded HEP lowers the H_2 evolution efficiency.[30] Moreover, IO_3^- reduction involves a six-electron transfer, requiring a cocatalyst loaded onto the OEP. These disadvantages of the IO_3^-/I^- redox mediator limited the choice of visible-light responsive OEP employed for a Z-scheme demonstration. The I_3^- shows parasitic photoabsorption of the visible light up to nearly 500 nm, thereby lowering the water splitting activity. Whereas, Fe^{3+}, I^- and IO_3^- show no significant absorption in the visible region.[17]

Gaseous product separation, enabled by the use of a liquid redox mediator, is essential for large-scale application of photocatalytic water splitting reaction with significantly improved STH conversion efficiency. Thus, here we discuss the advantages and disadvantages of Z-scheme overall water splitting using two photo-absorbers and different shuttle mediators. It is important properly design a corresponding photocatalytic reactor concept and to choose the appropriate combination of photocatalysts and redox mediators for maximized performance. Here, we analyze three conceptual types of suspension reactor designs and provide theoretical maximum efficiency calculations in order to quantify their limits and provide guidance for the best choice of photocatalyst materials and redox mediators.

3. Reactor design concepts and configuration

3.1 Design overview of conceptual photocatalytic particle suspension reactors

We broadly classify conceptual photocatalytic suspension reactors into three categories (Fig. 2) based on the possibility or inability to separate the produced hydrogen and oxygen gases, based on their ability to implement a Z-scheme (or dual absorber scheme), and based on the possibility to introduce wires that enable the operation of two different reaction environments (i.e. two different redox mediator) for OEP and HEP. Additionally, we also show analogous designs that consider immobilized photocatalysts on a conducting substrate (sometimes referred to as catalyst sheets), i.e. approaches that use solid mediators and no suspension.[31] The three types include: (i) a single photocatalyst reactor (type 1), (ii) a membrane-separated dual compartment reactor (OEP and HEP compartments) (type 2), and (iii) a membrane-separated dual compartment reactor (OEP and HEP compartments) with wire and two

auxiliary electrodes (type 3). Type 1 reactors lead to cogeneration of hydrogen and oxygen gases at one photocatalyst particle or a complex multicomponent particle (version type 1*). The multicomponent particles in type 1* are essentially a tandem multijunction light absorber, effectively made of two photocatalysts in direct contact or joined by a solid mediator. However, it cannot be guaranteed that the particles are always in the right orientation with respect to the light (i.e. larger bandgap material is hit by the light before the smaller bandgap material). Type 2 reactors consist of a HEP suspension compartment on top and OEP suspension compartment on bottom (or vice versa, OEP on top and HEP on bottom), with the oxidized and reduced forms of the redox mediator couple (Med_{ox}/Med_{red}) transported between the membrane-separated compartments. We refer to the configurations as HEP/OEP on top and OEP/HEP on bottom when indicating that the two compartment act as tandem photoabsorber that are optically in series (top compartment is hit first by the light). A subtype of reactor type 2 (type 2*) includes a version without membrane, effectively consisting of two particle types (OEP and HEP) mixed in solution in a single compartment. Types 1 and 2 require the photocatalyst(s) to operate in the same solution (with type 2 resulting in a small concentration gradient over the membrane) while type 3 enables the utilization of two different solutions separated by an ion-selective semipermeable membrane. The membranes in type 2 and 3 are non-permeable for hydrogen and oxygen to suppress or minimize any product crossover. The membrane in type 2 is required to be permeable for protons (in acidic conditions) and the oxidized and reduced forms of the mediator. The membrane in type 3 only requires permeability for protons (in acidic conditions) while suppressing the crossover of the respective mediator species. Type 3 reactors with HEP suspension compartment on top and OEP suspension compartment on bottom (or vice versa) are connected by a wire (for example a copper wire with platinum coils) that directly transport the electrons. The reduced and oxidized forms of the two redox couples (Med 1/Med 1_{ox} of the HER compartment and Med 2/Med 2_{red} of the OER compartment) are regenerated at the wire. This provides more flexibility in terms of acceptable reaction environment for the photocatalyst, however at the expense of additional reactions and the corresponding overpotentials.

3.2 Reactor type 1 – photocatalyst particle suspension reactor

Reactor type 1 is generally used in laboratory scale experimentation but its practical relevance is limited. A single photocatalyst particle (or two photocatalysts joined by a solid mediator resulting in a complex multicomponent particle) is used to split water to evolve hydrogen and oxygen in one (or two-step) photo-excitation. This kind of reactor will result in the production of hydrogen and oxygen gases in close vicinity and an explosive mixture in the headspace can build up. Proper separation approaches are needed for large scale application in order to ensure reactor safety and no loss in product yield.
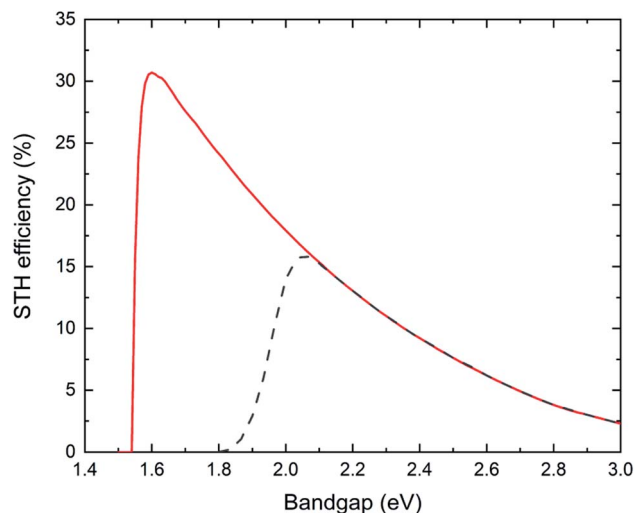
Fig. 3 Limiting STH efficiency as a function of the varying photocatalyst bandgap energy for type 1 reactor with single photocatalyst absorber. The red line shows the ideal case without any overpotentials, the black dashed line shows the non-ideal case with overpotentials.

Fig. 3 shows results of calculations of the (thermodynamic) limits of the solar-to-hydrogen efficiency, utilizing the detailed balance limit (*i.e.* Shockley–Queisser limit) to describe the charge absorption and separation (considering only radiative recombination) in the single photocatalyst particle reactor type 1. Two cases are considered: (i) the ideal case which assumes no kinetic, ohmic or mass transport overpotentials, and (ii) the more realistic case (termed non-ideal case) which considers kinetic and transport losses.[16] We observe a maximum STH efficiency of 30.6% (ideal case) with a photocatalyst having a bandgap of 1.6 eV, which generates just sufficient photovoltage to provide the required 1.23 V to split water. The steep drop in efficiency with lower bandgaps (<1.6 eV) is due to the insufficient photovoltage, while the efficiency decrease for larger bandgaps is a result of decreasing photocurrent. If kinetic and transport losses are considered (non-ideal case), the peak efficiency is at 16% for a bandgap of 2.1 eV.

The most efficient experimental demonstration has been reported by Takata *et al.*[11] using SrTiO$_3$:Al (bandgap energy: 3.2 eV) with a STH efficiency of 0.65%. At this bandgap energy, the calculated maximum theoretical efficiency (for the ideal case) is 1.3%. Another oxysulfide material, Y$_2$Ti$_2$O$_5$S$_2$ (bandgap energy 1.9 eV) has been reported to be active for one-step overall water splitting, with a measured STH efficiency of 0.007%.[32] The theoretical limiting STH efficiency at the bandgap of 1.9 eV is 20.9% and 2.9% for the ideal and non-ideal case, respectively.

If a complex multicomponent particle (made of two different photoabsorbers with solid mediator) is considered (type 1*) and a top-bottom arrangement of all the multicomponent particles can be ensured (*i.e.* the photocatalyst with larger bandgap receiving the solar radiation before the second photocatalyst with the lower bandgap), the theoretical maximum STH efficiency can be as high as 40% (ideal case) when using

photoabsorbers with bandgaps of 1.4 eV and 0.52 eV (ref. 16) and reduces to 29% (non-ideal case) with bandgaps of 1.6 eV and 0.95 eV.[33]

The limiting efficiencies of the suspension reactors and catalyst sheets for types 1 and 1* are equal. However, it is expected that the charge separation in the catalyst sheet configuration is more effective, given the contact with the conducting layer might induce a stronger, migration supported charge separation.

3.3 Reactor type 2 – membrane-separated dual compartment reactor (OEP and HEP compartments)

Type 2 reactor comprises of two different photocatalyst particles: the OEP promotes the oxygen evolution and the mediator reduction, and the HEP promotes the hydrogen evolution and the mediator oxidation. The electrolyte needs to allow for the transport of mediator species between the OEP and HEP and for the transport of protons (in the case of an acidic environment). To enable product separation, the two particle types are suspended in separate compartments, separated by a semipermeable membrane. The membrane should allow for the transport of the reduced and oxidized form of the redox mediator species along with protons or hydroxide ions that are produced at the OEP in acidic conditions or at the HEP in alkaline conditions. The membrane should be impermeable for hydrogen and oxygen to prevent mixing of products.[34] This kind of reactor needs a combination of two different photocatalysts that are sufficiently active toward hydrogen and oxygen evolution reactions and towards mediator oxidation and reduction reactions, respectively. Type 2 (and type 3) systematically allow for the utilization of a Z-scheme and, in the case that one compartment is on top of the other (*i.e.* optically in-series with respect to the solar irradiation), a dual absorber approach is realized. This kind of reactor has the promise to allow for the use of a wide variety of photocatalysts with narrow bandgap energies modified with suitable co-catalysts to promote the various surface chemical reactions. A Z-scheme water splitting reaction with two photocatalysts can also be carried out in a single compartment without any membrane (design version type 2*) but this does not allow for separation of product gases and is not a safe practical reactor design. However, type 2* is more often used in lab-scale demonstrations.

Fig. 4 shows results of calculations of the (thermodynamic) limits of the solar-to-hydrogen efficiency of reactor concept type 2. We used a unsteady adaptation of the equivalent circuit model with the detailed balance limit for the photo absorber and concentration-dependent electrochemical load (see ESI† for details on the modeling approach) to understand how the choice of the OEP's and HEP's bandgap and the choice of the redox mediator equilibrium potential is affecting the limiting efficiencies.[8] The transient model solves for species transport and mass conservation in the two membrane-separated reactor compartments. Again, an ideal case without transport and kinetic losses is considered as well as a non-ideal case with species concentration-dependent reaction overpotentials and ohmic losses.
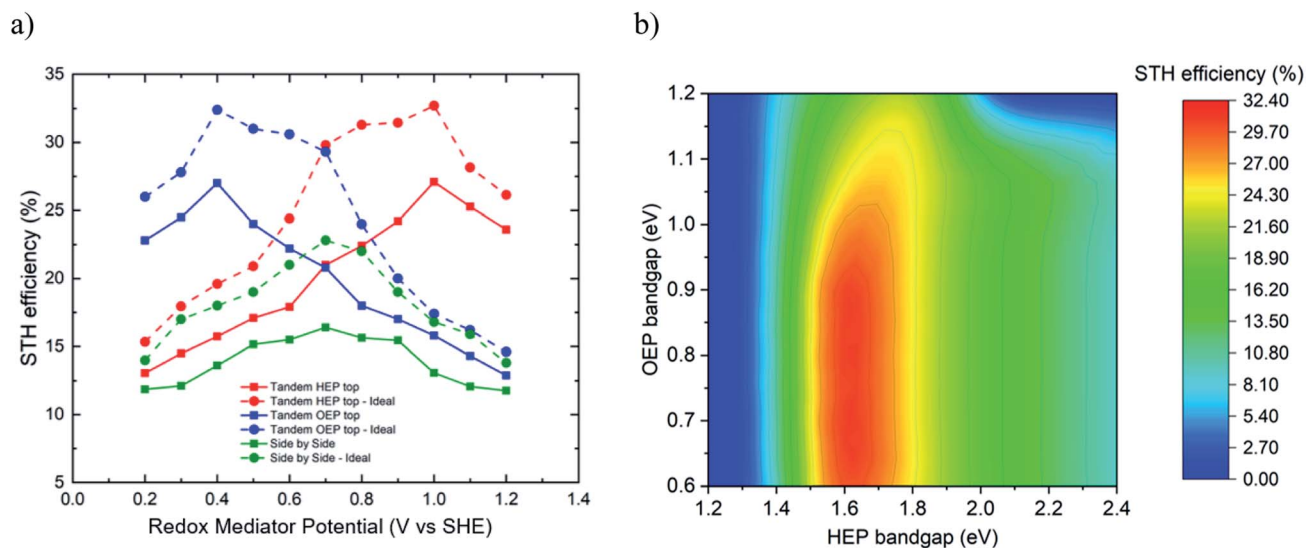
a)

b)

Fig. 4 (a) Variation of maximum STH efficiency (%) with redox mediator potential (V *vs.* SHE) plot for the side by side (green) and tandem configuration alternatively with HEP (red) or OEP (blue) on top. The dashed and solid lines indicate the ideal case (no overpotentials) and non-ideal case (with overpotentials), respectively. (b) STH efficiency (%) as a function of the HEP's (*x*-axis) and OEP's (*y*-axis) bandgap energy in ideal top–bottom configuration (in terms of optical arrangement) with HEP on top at redox mediator potential of 1.0 V *vs.* SHE.

Fig. 4a presents for the two cases the limiting efficiencies for two different type 2 reactor designs: (i) separated chambers side-by-side arrangement, and (ii) separated chambers top-bottom arrangement (in terms of optical arrangement) with either HEP chamber on top or OEP chamber on top. A maximum STH efficiency of 32.4% for ideal case and 27.1% for non-ideal case is observed for the top-bottom configuration at a redox mediator potential of 1.0 V *vs.* SHE (if HEP on top) and 0.4 V *vs.* SHE (if OEP on top). The corresponding choice of HEP/OEP bandgap energies for the ideal case are 1.6 eV/0.8 eV (if HEP on top, Fig. 4b) and 0.8 eV/1.6 eV (if OEP on top). The bandgap combinations for the non-ideal case are 1.75 eV/1.0 eV (if HEP on top) and 1.0 eV/1.75 eV (if OEP on top). It was observed that the bandgap energy of the HEP was more strictly limited to a range of 1.55 to 1.7 eV to ensure high STH efficiency, while for the bottoming OEP particle a bandgap range of 0.6 to 0.95 eV was acceptable. This bandgap range is varying with the equilibrium potential of the redox mediator. For an equilibrium potential of redox mediator of x V *vs.* SHE, the minimal electrochemical load for the HEP is x V–E_{HER}, whereas the minimal electrochemical load for the OEP is E_{OER}–x V, see in Fig. 1b. Thus, depending on the redox mediator, either the HEP or the OEP has to sustain a larger electrochemical load, deciding if HEP or OEP should ideally be placed on top. Higher electrochemical loads have to be provided by choosing a larger bandgap, generating larger photovoltage at the expense of lower photocurrent and, in turn, lower STH efficiencies. For the HEP on top configuration, increasing the redox mediator potential from 0.2 to 1.0 V *vs.* SHE, the optimal HEP/OEP bandgap energies vary from 2.2/1.55 eV to 1.6/0.8 eV, respectively.

The side-by-side configuration achieved a maximum STH efficiency of 23% for the ideal case and 16.8% for the non-ideal case at a redox mediator potential of 0.7 V *vs.* SHE. Bandgap

energy combinations allowing to achieve such an efficiency are within 1.2 to 1.3 eV for both, HEP and OEP for the ideal case and at 1.4 eV for the non-ideal case. From a modelling approach, the limiting STH efficiencies of the reactor type 2* (*i.e.* the two-particle reactor without membrane) can be approximated by the side-by-side configuration, indicating an efficiency limit of 23%. The efficiency limiting calculations indicate that the conceptual design choice (side-by-side, membrane-less version, top-bottom with HEP on top, top-bottom with OEP on top) is affecting the choice of OEP and HEP bandgaps and redox mediator potential that lead to the maximum STH efficiencies.

The most efficient experimental demonstration has been reported by Qi *et al.*[35] using the system (Pt/ZrO$_2$/TaON)–[Fe(CN)$_6$]$^{3-}$/[Fe(CN)$_6$]$^{4-}$–(Au NPs/CoO$_x$/BiVO$_4$) (bandgap energies of HEP and OEP: 2.4 eV, mediator potential of 0.356 V *vs.* SHE) with a STH efficiency of 0.5%. At this bandgap and mediator combination, the maximum theoretical efficiency would be 4.9%.

Z-Scheme water splitting with a solid redox mediator has also been investigated using, for example, a particulate photocatalyst sheet with gold as solid back contact layer mediating e$^-$ transfer between OEP and HEP (Fig. 2).[36,37] In this case, the mediator is essentially creating an ohmic contact with the two photocatalysts. The theoretical maximum STH efficiency for the ideal case of a catalyst sheet can be calculated based on a dual-absorbing photoelectrochemical device, with a peak STH efficiency of 40% when using photoabsorbers with bandgaps of 1.4 eV and 0.52 eV,[16] which reduces in a non-ideal case and the larger distance between the particle types, but is typically larger than the top-bottom arrangement of the suspension reactor (peak efficiency of 32.4%). However, this is only true if the two absorbers are in-series (in terms of light path), while it is more likely that a side-by-side arrangement is generally achieved on

a catalyst sheet. In this side-by-side arrangement, the theoretical limiting efficiency for a catalyst sheet is 15.3% (*i.e.* 30.6% for a single absorber divided by two, given that double the area is needed), which is inferior to the side-by-side design of the suspension reactor (peak efficiency of 23%).

3.4 Reactor type 3 – membrane-separated dual compartment reactor (OEP and HEP compartments) with wire and two auxiliary electrodes

Type 2 and type 3 reactors allow for product separation as water oxidation and reduction reactions take place in two different compartments which are separated from each other by a semi-permeable ion exchange membrane. The advantage of type 3 reactor is that it gives extra flexibility in terms of redox mediator choice in the HEP or OEP compartments, as the mediator can be different. The chambers communicate through the selective transport of protons (in an acidic example) through the membrane and electron transport in the wire connecting the two auxiliary electrodes (for example made of Pt). The membrane's only function is to allow the transportation of protons (or hydroxyl ions in the alkaline case) between the two chambers while preventing the mediator species from passing or products (hydrogen and oxygen) from crossing over. Nafion is a widely employed proton exchange membrane which satisfies the condition of proton conduction and prevents product crossover, however less is known about Nafion's specific transport properties with respect to the different mediator species.[34,38]

To maintain the operating Z-scheme in type 3, the equilibrium potential of the redox mediator in the HEP compartment should be more positive compared to the equilibrium potential of the redox mediator of the OEP compartment. Additionally,

the equilibrium potential of the redox mediator operating in the OEP compartment must be more positive than the CBM of the OEP, and the equilibrium potential of the redox mediator in HEP compartment must be more negative than VBM of the HEP. Thus, this type 3 reactor can maintain a Z-scheme and drive the HER and OER. The type 3 however has added overpotentials due to the two extra sets of redox reactions and additional ohmic losses due to the electrodes. Type 3 essentially trades off additional losses and overpotentials for flexibility in material choice.

The limiting efficiency calculations predicted for the conceptual reactor type 3 a maximum STH efficiency of 30.2% for ideal case and 24% for non-ideal case at a redox mediator potential of 1.0 V *vs.* SHE (for HEP on top) and 0.4 V *vs.* SHE (for OEP on top), respectively (Fig. 5a). For the ideal case, the bandgap combination of 1.65 eV for HEP (on top) and 0.8 eV for OEP at redox mediator potential of 1.0 V *vs.* SHE for OEP compartment lead to best performance (Fig. 5b). For OEP on top, bandgaps of 0.8 eV for HEP and 1.65 eV for OEP at redox mediator potential of 0.4 V *vs.* SHE led to the best performance. A reasonable range of bandgaps enabling a high efficiency is 1.6 to 1.8 eV for the top light absorber and 0.6 to 1.1 eV for the bottom light absorber. For both cases, the performance is relatively insensitive to the redox mediator potential of the top chamber as long as it maintains the Z-scheme. In the non-ideal case, the maximum STH efficiency of 24% was observed at a bandgap combination of 1.8 eV for HEP (on top) and 1.2 eV for OEP at redox mediator potential of 1.0 V *vs.* SHE for OEP compartment.

A practical demonstration of the type 3 reactor has been reported by Matsumura *et al.*[38] where they used Pt loaded TiO$_2$ and rutile TiO$_2$ as HEP and OEP, respectively, in presence of
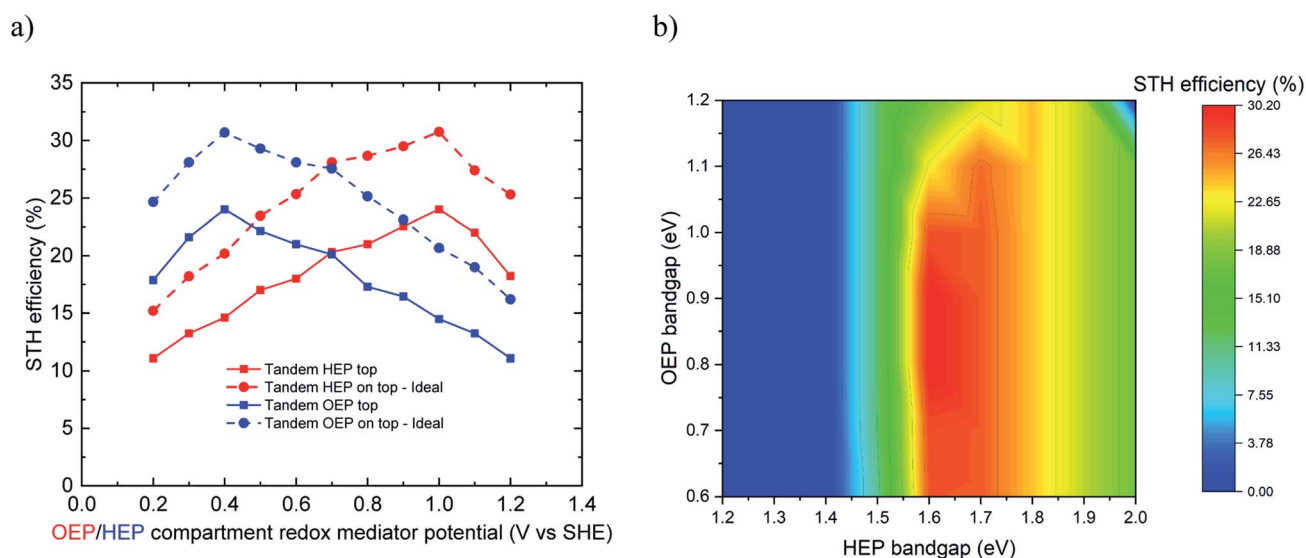

Fig. 5 (a) Variation of maximum STH efficiency (%) with OEP/HEP compartment redox mediator potential (V *vs.* SHE) in tandem configuration with HEP (red) or OEP (blue) on top. The dashed and slide lines indicate the ideal case (no overpotentials) and non-ideal case (with overpotentials), respectively. (b) STH efficiency (%) as a function of the HEP's (*x*-axis) and OEP's (*y*-axis) bandgap energy in top-bottom configuration (in terms of optical arrangement) with HEP on top at redox mediator potential of OER compartment of 1.0 V *vs.* SHE (redox mediator of HER is insensitive).

Br^-/Br_2 and $Fe^{3+/2+}$ as HEP and OEP compartment redox mediators, respectively. This system achieved an AQY of 17% (*ca.* 0.2% STH). They performed water reduction reaction using suspended Pt–TiO_2 particles where Br^- ions were oxidized to Br_2 in the H_2 compartment and rutile TiO_2 was used for water oxidation where Fe^{3+} ions were reduced to Fe^{2+} ions in the O_2 compartment. These two sets of reactions were carried out in separate compartments and connected *via* platinum electrodes and a proton exchange membrane. Protons were transported through the membrane to maintain electroneutrality and the pH of the solutions in the two compartments. The maximum theoretical STH efficiency for such a system of HEP and OEP bandgap energies of 3.0 eV (for TiO_2) and redox mediator equilibrium potentials of 0.77 and 1.08 V *vs.* SHE, respectively, is 1.2%.

3.5 Losses in practical reactors

The theoretical assessment of the reactor concepts in the sections above does not consider more realistic losses due to, for example, the multi-dimensional nature of the processes and the resulting heterogeneities in the variable fields (light intensity, concentrations, *etc.*). As the detailed quantification of these more realistic optical, charge and mass transport losses will depend on the exact choice of material, operating condition as well as architecture and geometrical dimension, we do not consider it here as we aim at the identification of broad reactor concepts and the formulation of general design guidelines. We refer to two example studies of photocatalytic devices considering details of these practical losses by Cassano *et al.*[41] and Bala Chandran *et al.*[20] However, we discuss some of the expected

effects of specific dimensional choices and resulting heterogeneities. For example, a back of the envelope calculation indicated that the heterogeneity in light absorption (*i.e.* the exponential decrease in local intensity) can reduce the height-averaged efficiency by a factor of 4 (assuming an optical thickness of 5). The optical thickness is a function of particle size, geometry, solution concentration, solution parasitic absorption, reactor dimension *etc.* The photocatalyst particle size however does not only influence the absorption and scattering of light, but also the charge carrier separation. Cating *et al.*[39] indicated that smaller diameter photocatalysts exhibit shorter recombination lifetimes and recombination velocities. Typically, the photocatalyst particles are a mixture of particles with sizes of a few hundred nanometers and particle agglomerates of micrometer size. The ideal particle size is a tradeoff between desired large sizes that are able to support the space charge region and exciton separation but also small sizes that facilitate fast charge collection. On a reactor level, without varying the size of the particles, the optical absorption of particle suspensions can be adjusted by changing the particle concentration and/or vessel height. Absorption of nearly all incident above-bandgap sunlight is possible with appropriate choice of particle concentration and/or vessel height (if the electrolyte parasitic losses are small). Thus, the volume of the electrolyte used in a particle suspension reactor dictates the amount and size of light-absorber material. Bala Chandran *et al.*[20] discuss the effects of optical properties of the semiconductor and redox shuttle species on the system performance for a baseline STH efficiency of 1%. They highlight the effect of optical thickness of the semiconductor particles on the performance which is
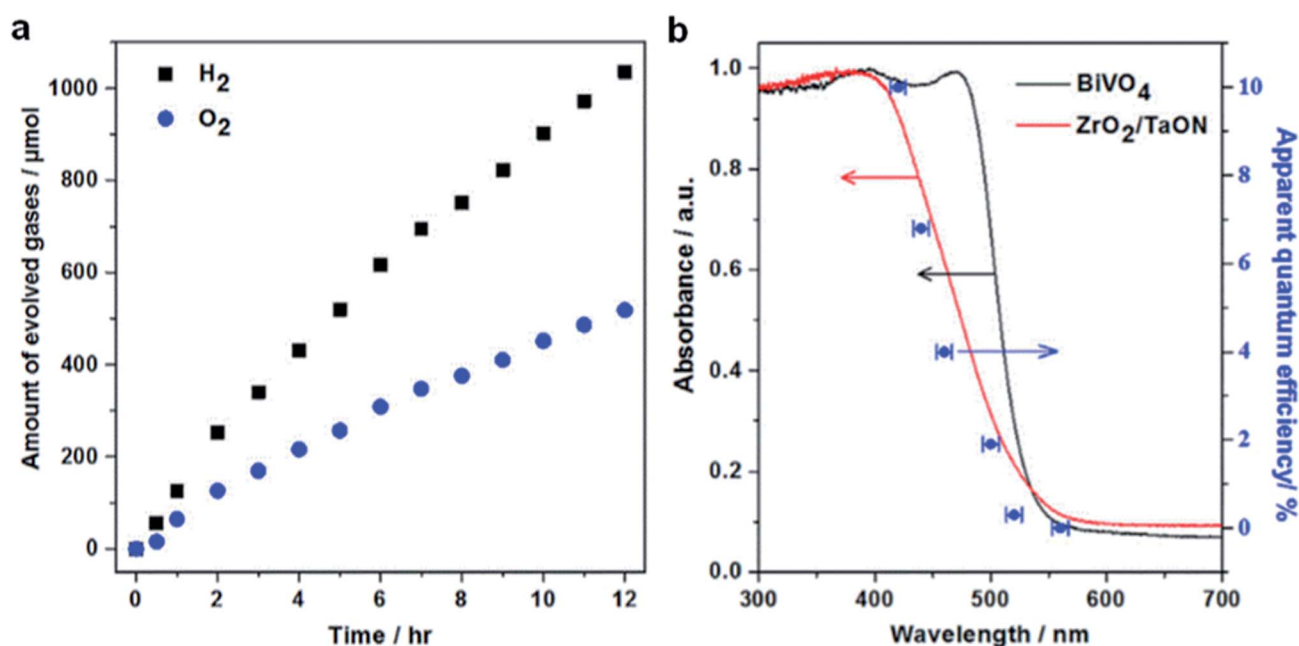

Fig. 6 (a) Time courses of Z-scheme overall water splitting and (b) variation of AQY as a function of irradiation wavelength for the combination $(Pt/ZrO_2/TaON)$–$(Fe(CN)_6]^{3-}/[Fe(CN)_6]^{4-})$–$(Au\ NPs/CoO_x/BiVO_4)$. Reaction conditions: 75 mg OEP (0.8 wt% Au; 0.1 wt% CoO_x), 75 mg HEP (1.0 wt% Rh, 1.5 wt% Cr), 150 mL 25 mM sodium phosphate buffer solution (pH 6.0) containing $K_4[Fe(CN)_6]$ (10 mM), 300 W Xe lamp ($\lambda \geq 420$ nm), temperature 298 K, Pyrex top-irradiation type. Reprinted with permission from ref. 35. Copyright 2018 Elsevier Inc.

linearly dependent on the particle concentration, absorption coefficient, the particle cross section and the reactor height. The performance increased with increase in optical thickness limited then by the particle band gap and spectral absorptivity. They concluded that due to parasitic light absorption of species like I_3^-/I^- and Fe^{3+}/Fe^{2+} the concentrations of these species should be kept prohibitively low (<5 mM), thus promoting Q/QH_2 and IO_3^-/I^- as better alternatives in the interest of the optical behavior. The optimum optical performance is strongly influenced not only by the choice of the semiconductor particles in the two reaction compartments, but also by the type and concentration of the redox shuttle species considered. Particle sedimentation and the accumulation of contaminants (for example degradation products) over time might further change the optical characteristics of the reactor.

Another major technical challenge in reactor operation is maintaining a sufficient flow, concentration and conductivity (ionic strength) of the electrolyte. The concentration gradients of the redox shuttle should be kept minimal to avoid related overpotentials. Mass transport of redox shuttles (as well as reactant and protons/hydroxyl ions) in particle suspension reactors occurs across and between compartments by forced convection (mixing), natural convection, and diffusion. Ionic migration of charged redox shuttles and proton (or hydroxyl ions) can happen across and between the compartments. In reactors with membranes, the mass transport resistance for the redox shuttle across the membrane would limit the reactor efficiency, thus a tailored membrane for the redox shuttle should be considered. Slow redox-shuttle transport throughout the reactor results in significant additional thermodynamic potential requirements and concentration overpotentials.[40] Contaminants potentially affect the membrane conductivity and solubility. Additionally, contaminants and degradation products are expected to have an effect on the catalyst performance and kinetics. Cassano et al.[41] studied the possibility of mass transport limitations in the bulk of photocatalytic suspensions of pure titanium dioxide. They concluded that concentration profiles in the bulk will be always present unless very good mixing conditions in the characteristic direction of radiation propagation are used. They conclude that in flow reactors, when fully developed turbulent flow operation is achieved, the mass transfer limitations are almost negligible. This is supported by their case when the photocatalytic reaction is not fast, employing TiO_2 mass concentration below 1 g L^{-1}, incoming irradiation rates below 1.0×10^{-7} einstein cm^{-2} s^{-1} and very good mixing conditions, the mass transport limitations in the bulk of slurry photocatalytic reactors are not important. The conceptual reactor design (tandem or side-by-side configuration) will also influence the main direction of mass transport of species (with respect to the irradiation direction) and either enhance (in tandem) or reduce (side-by-side) the gradients.

4. Materials review for Z-scheme overall water splitting using water soluble and solid mediators

We discuss the materials typically used for Z-scheme overall water splitting using liquid redox mediators (summarized in
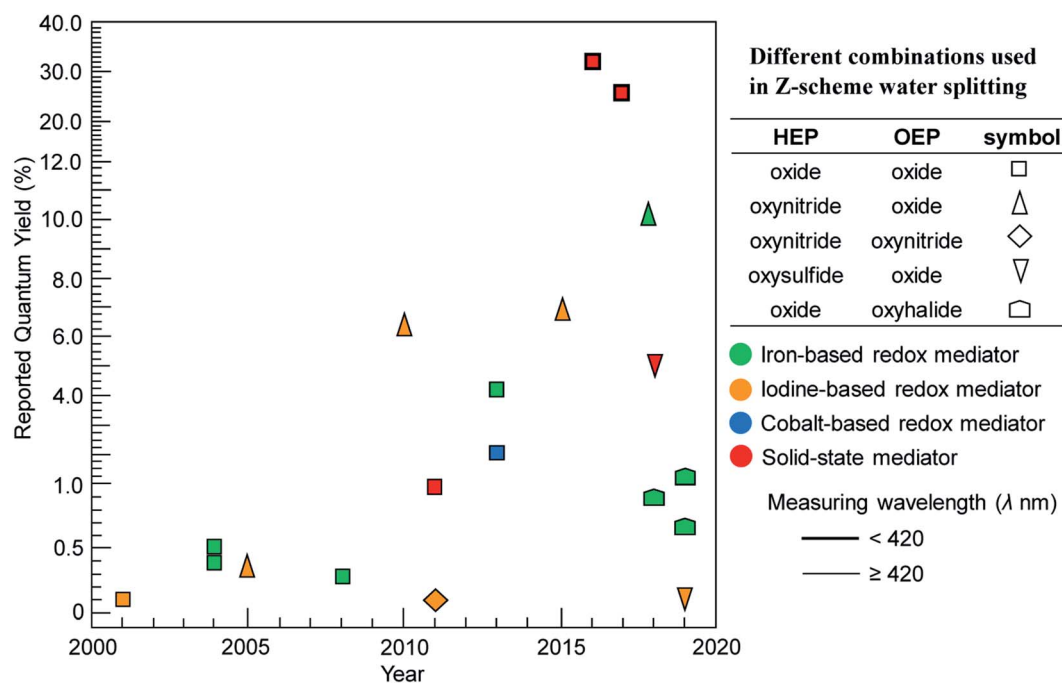

Fig. 7 Maximum reported quantum yields over the last 20 years for visible-light driven Z-scheme overall water splitting using powder suspensions categorized by type of photocatalysts (shape), shuttle mediator (color) and measuring wavelength (border thickness). Figure is an updated version of Fig. 9 in ref. 40.

Table 1), summarize demonstrations of overall water splitting, and discuss these materials and demonstrations in the light of the theoretical efficiency calculations (chapter 3). Our main focus lies on Z-scheme approaches that utilize different combinations of HEPs and OEPs with an appropriate redox mediator (reactor types 2 and 3), designs that could lead to high STH efficiencies while ensuring spatially-separated production and collection of the product gases. Metal oxides such as WO_3, $BiVO_4$ and (oxy)halide, have been widely used as OEP, whereas $SrTiO_3$, (oxy)nitrides and (oxy)sulfides are more common for HEP.

$SrTiO_3$ (STO) has been reported as HEP in combination with an OEP in a Z-scheme configuration for overall water splitting under sunlight. Sayama et al. reported overall water splitting for $(Pt/STO:Cr,Ta)–(IO_3^-/I^-)–(PtO_x/WO_3)$, considered as one of the first demonstrations under visible light irradiation.[42] Co-doping of Rh^{3+} and Sb^{4+} onto STO (STO:Rh/Sb) with a specific ratio was reported to work as OEP. A Z-scheme overall water splitting system was constructed as a combination of $(Ru/STO:Rh)–(Fe^{3+}/Fe^{2+})–(IrO_x/STO:Rh/Sb)$ operating under visible light.[43] Rh-

doped STO (STO:Rh) modified with Ru or Pt as cocatalyst has been widely used as HEP to construct a Z-scheme in combination with OEPs such as BVO, $BiMoO_6$, or WO_3 using different liquid electron mediators (for e.g. IO_3^-/I^-, Fe^{3+}/Fe^{2+}, $[Co(bpy)_3]^{3+/2+}$, $[Co(phen)_3]^{3+/2+}$) to maximize the overall water splitting efficiency. Kudo and co-workers utilized the combination $(Pt/SrTiO_3:Rh)–(Fe^{3+}/Fe^{2+})–(BVO)$, achieving an AQY of 0.3% at 440 nm, larger than what was achieved when utilizing $BiMoO_6$ or WO_3 as OEP.[44] They synthesized STO by a solid-state reaction (SSR). The same group of authors also synthesized STO:Rh by hydrothermal (HT), polymerized complex (PC) methods.[45] The Z-scheme overall water splitting activity was found to improve significantly when Pt/STO-HT:Rh and Pt/STO-PC:Rh were used as HEP in combination with BVO, reaching an AQY of 3.9–4.2% at 440 nm. STO synthesized by HT and PC methods showed to be efficient in preventing the backward reaction (water from evolved H_2 and O_2 gases) while this was not successful for SSR synthesized STO. Metal-complex based Z-schemes of $(Ru/SrTiO_3:Rh)–(Co-complex)–(OEP)$ were studied by Kudo et al.[46] WO_3 and $TiO_2:Cr,Sb$ as OEP showed lower and
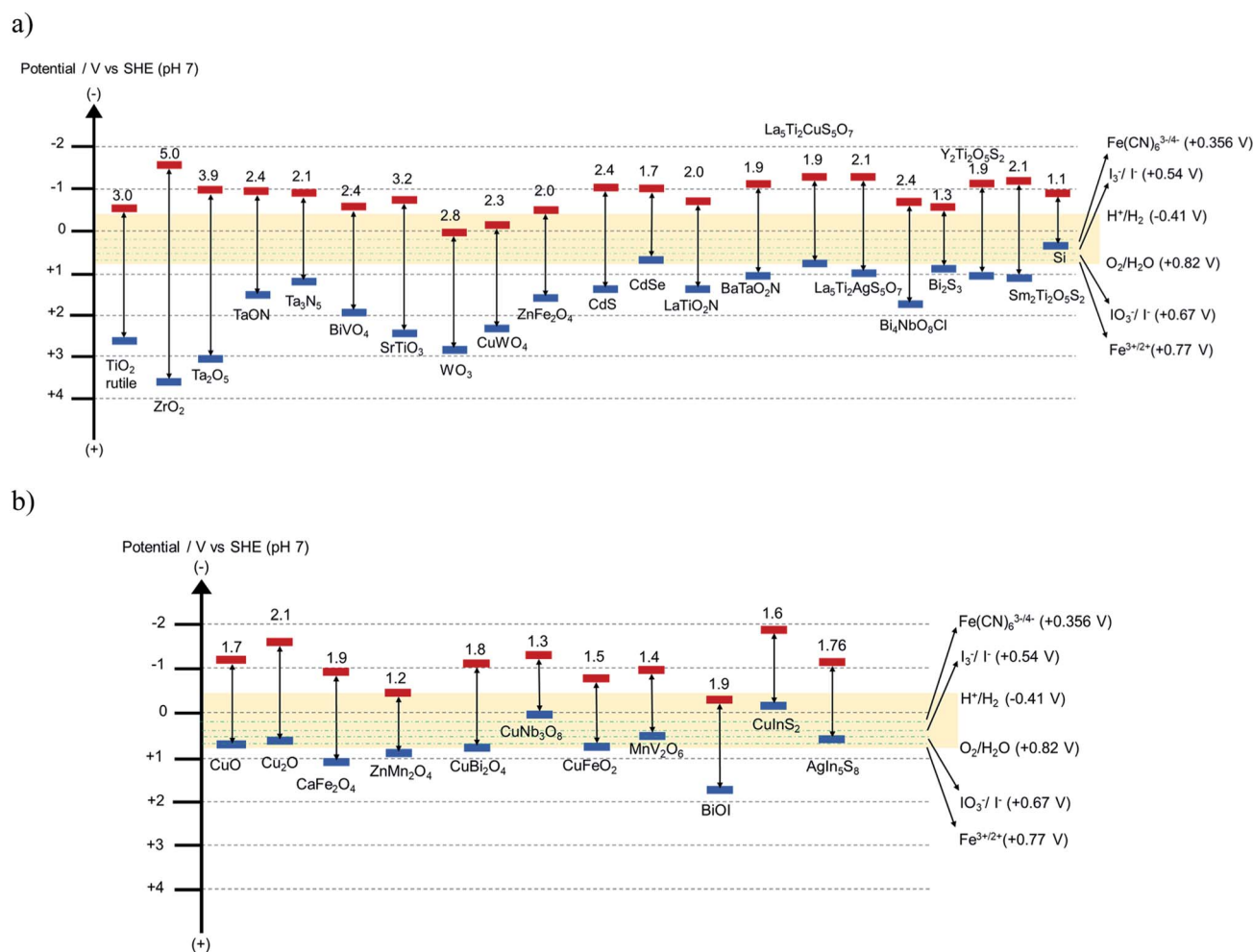

Fig. 8 Schematic band diagram of some known (a) n–type and (b) p–type semiconductors. Data for $La_5Ti_2CuS_5O_7$ and $BaTaO_2N$ are obtained from ref. 65 and 66. The yellow horizontal range indicates the redox potentials of OER and HER, and the dotted green horizontal lines indicate the redox potential of typical redox mediators.

non-stoichiometric O_2 evolution, whereas combination with BVO showed higher and stoichiometric gas evolution at a steady rate for a duration of 16 h. In their study, the (Ru/SrTiO$_3$:Rh)–(Co-complex)–(BVO) Z-scheme was constructed using $[Co(bpy)_3]^{3+/2+}$ and $[Co(phen)_3]^{3+/2+}$ as electron mediators and the HEP and OEP chambers were divided by a separator to isolate the product gases.

(Oxy)nitride photocatalysts, utilizing a large portion of the visible light, are known to function as both, HEP and OEP, depending on the energy level of VB and CB. Pt-loaded TaON as HEP was combined with PtO_x/WO_3 as OEP in an aqueous solution of IO_3^-/I^-. This (Pt/TaON)–(IO_3^-/I^-)–(PtO_x/WO_3) combination produced stoichiometric evolution of H_2 and O_2 for 60 h, achieving an AQY of 0.4% at 420 nm.[50] Whereas, ZrO_2 modified TaON employed as HEP in an (Pt/ZrO$_2$/TaON)–(IO_3^-/I^-)–(PtO_x/WO_3) Z-scheme system achieved an AQY of 6.3% at 420 nm. The modification of the TaON surface with ZrO_2 was effective in suppressing the formation of reduced Ta-species (Ta^{3+} or Ta^{4+}) and anionic defects during the nitridation (both are known to act as charge recombination centers) and thereby achieved improved overall water splitting activity.[51] In 2018, (Pt/ZrO$_2$/TaON)–($[Fe(CN)_6]^{3-}/[Fe(CN)_6]^{4-}$)–(Au NPs/CoO$_x$/BiVO$_4$) was reported operating at an AQY of 10.3% at 420 nm (Fig. 6) and an STH efficiency of 0.5% (the highest STH efficiency achieved with a water soluble redox mediator).[35] The water splitting efficiency was drastically enhanced by the site-selective deposition of Au nanoparticles (NPs) and CoO$_x$ cocatalysts on the e$^-$-rich {010} and h$^+$-rich {110} facets of BiVO$_4$, enabling efficient transfer of e$^-$ from the Au NPs to $[Fe(CN)_6]^{3-}$.

TaON has also been found to be active as both HEP and OEP. For instance, the combination of (Pt/ZrO$_2$/TaON)–(IO_3^-/I^-)–

(RuO$_2$/TaON) achieved stoichiometric gas evolution at a rate of 8.0 μmol h^{-1} and 4.0 μmol h^{-1} for H_2 and O_2, respectively, under visible light.[52] Ta-based oxynitrides, ATaO$_2$N (A = Ca, Sr, Ba), have been utilized as HEP in combination with PtO_x–WO_3 as OEP under visible light in the presence of an IO_3^-/I^- redox shuttle. (Pt/BaTaO$_2$N)–(IO_3^-/I^-)–(PtO_x/WO_3) is considered the first example of overall Z-scheme water splitting utilizing visible light with wavelengths longer than 600 nm for the H_2 evolution.[53] This system achieved an AQY of 0.1% at 420–440 nm, lower than the TaON based systems. The system based on Pt/SrTaO$_2$N failed to work as a Z-scheme due to the self-oxidative photo corrosion detected in the form of gaseous N_2. Maeda *et al.* studied the BaZrO$_3$–BaTaO$_2$N solid solution as HEP in a Z-scheme for overall water splitting.[54] This photocatalyst has a narrow bandgap energy of 1.8 eV, absorbing photons in the visible light region up to 660 nm. A Pt loaded solid solution of BaZrO$_3$–BaTaO$_2$N was also utilized as the HEP in combination with either PtO_x/WO_3 or TiO_2 (rutile) as the OEP in the presence of an IO_3^-/I^- redox shuttle. The (Pt/BaZrO$_3$–BaTaO$_2$N)–(IO_3^-/I^-)–(PtO_x/WO_3) system achieved an H_2 and O_2 evolution activity of 22.4 and 9.3 μmol h^{-1}, whereas the (Pt/BaZrO$_3$–BaTaO$_2$N)–(IO_3^-/I^-)–(TiO_2) system evolved H_2 and O_2 gas at a rate of 21.3 and 9.4 μmol h^{-1} with a STH of 0.0067% and 0.014%, respectively. These STH efficiency calculations were made based on the gas evolution in the first three hours. Z-scheme overall water splitting for the system (MgTa$_2$O$_{6-x}$N$_y$/TaON)–(IO_3^-/I^-)–(PtO_x/WO_3) achieved an AQY of 6.8% at 420 nm.[55] This system utilized visible light up to 570 nm for water splitting and the formation of a heterojunction between the MgTa$_2$O$_{6-x}$N$_y$ and TaON photocatalysts was the key feature of this system. This heterojunction was effective in reducing the charge recombination
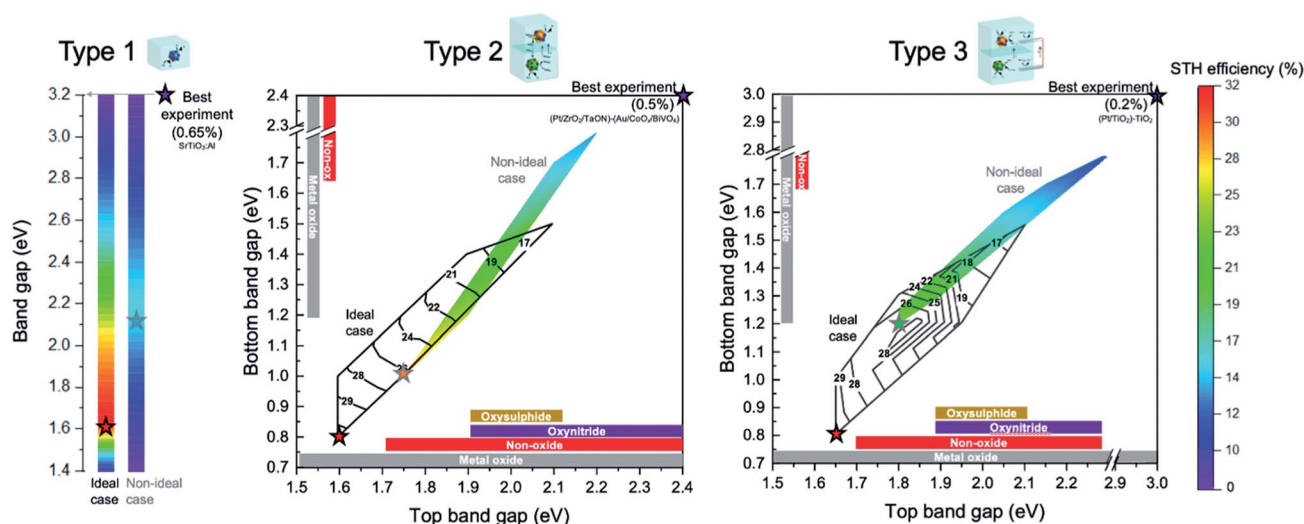

Fig. 9 Theoretical maximum efficiency ranges (color bar for quantification of STH efficiency is located on the extreme right and applies to all three types) as a function of band gap(s) of the involved semiconductor particle(s) for the three conceptual reactor design types (for ideal, no-overpotential case; or for non-ideal case that includes overpotentials). The best theoretical case for each type as ideal and non-ideal cases are indicated with stars. The most efficient laboratory-scale demonstration with their material combinations (located at their respective band gaps) are also indicated with a star (termed "best experiment"). The colored contour plot in type 2 and 3 indicate the non-ideal case and black iso-lines indicate the ideal case. For the theoretical predictions in type 2 and 3, the redox mediator potential is optimized for the particular band gap combination (see details in Fig. 4 and 5). Typical material types (oxysulphide, oxynitride, non-oxides and metal oxides) used in experiments and their band gap ranges are indicated by colored bars.

and defect density. As the electron transfer occurs from the CB of $MgTa_2O_{6-x}N_y$ to CB of TaON and holes transfer occurs from VB of TaON to VB of $MgTa_2O_{6-x}N_y$, charge carrier recombination was effectively suppressed by the heterostructure. Abe and co-workers have extensively studied Bi_4NbO_8Cl (BNOC), an oxychloride semiconductor with bandgap energy 2.4 eV, as OEP for Z-scheme overall water splitting in combination with Ru/STO:Rh as HEP using Fe^{3+}/Fe^{2+} as electron mediator under visible light. This combination initially achieved an overall water splitting activity of 15.0 μmol h^{-1} for H$_2$ and 7.0 μmol h^{-1} for O$_2$ using unmodified BNOC.[48] Flux assisted two-step synthesis of BNOC using excess halogen precursor with improved crystallinity and reduced halogen defects enhanced the Z-scheme overall water splitting efficiency for the combination (Ru/STO:Rh)–(Fe^{3+}/Fe^{2+})–(RuO$_2$/BNOC), achieving an AQY of 1.3% at 420 nm.[49] This AQY is still three-folds lower than what has been achieved using BIVO$_4$ as OEP under the same condition.

Among (oxy)sulfides, $Sm_2Ti_2O_2S_5$ was utilized for the first time as HEP in combination with rutile TiO$_2$ in presence of an IO$_3^-$/I$^-$ redox mediator. This combination requires UV light irradiation for the excitation of the TiO$_2$. Post-treatments of Pt-loaded $Sm_2Ti_2O_2S_5$ by sulphur annealing and nitric acid etching improved the H$_2$ evolution activity by several times in a Z-scheme compared to the unmodified $Sm_2Ti_2O_2S_5$. Post-treatments were necessary to remove Ti^{3+} species from $Sm_2Ti_2O_2S_5$ surface to suppress charge recombination. This combination achieved an H$_2$ and O$_2$ evolution activity of 9.0 and 3.2 μmol h^{-1}, respectively, calculated based on gas evolution in five hours.[56] Kudo and co-workers have studied a combination of metal sulfide Ru/(CuGa)$_{0.8}$Zn$_{0.4}$S$_2$ and BVO as HEP and OEP, respectively, in the presence of [Co(terpy)$_3$]$^{3+/2+}$ as redox mediator under visible light. This combination achieved an STH of 0.025% with H$_2$ and O$_2$ evolution activity of 3.1 and 1.6 μmol h^{-1}, respectively, for a duration of 16 hours.[57] In 2019, La$_5$Ti$_2$AgS$_5$O$_7$ co-loaded with Pt and NiS cocatalysts was utilized as HEP in combination with PtO$_x$/WO$_3$ as OEP, achieving an AQY of 0.12% at 420 nm in the presence of I$_3^-$/I$^-$ as redox mediator. This is the highest water splitting efficiency reported utilizing (oxy)sulfides as HEP in the presence of a water soluble redox mediator.[58]

Z-Schemes were also constructed using solid-state mediators, such as photo-reduced graphene oxide (PRGO), gold and carbon, to facilitate e$^-$ transfer between the HEP and OEP. A photocatalyst sheet with gold and carbon as conductive layer achieved an energy conversion efficiency higher than 1.0% for the combination of (CrO$_x$/Ru/STO:Rh,La)–(Au or C)–(BiVO$_4$:Mo), several times higher than what was achieved using PRGO.[59–61] All these STH efficiencies were obtained under reduced pressure (at 10 kPa) and at 331 K. Whereas at ambient pressure 1.0% STH was the highest in Z-scheme pure overall water splitting. However, this STH efficiency was double compared to what was obtained using a soluble redox mediator for the combination (Pt/ZrO$_2$/TaON)–(Fe(CN)$_6$]$^{3-}$/[Fe(CN)$_6$]$^{4-}$)–(AuNPs/CoO$_x$/BiVO$_4$).[35] Z-Scheme was also performed using non-oxide photocatalysts but the efficiency achieved was much lower compared to what achieved using metal oxides.[62–64] Z-Schemes

designed with solid-state mediators do only allow in a few designs for product separation, designs which effectively resemble traditional photoelectrochemical designs (see Fig. 2).

Reported AQY for different combinations of HEP, OEP and redox mediator over the last twenty years (2000–2020) are presented in Fig. 7. We considered only selected key results, providing a quick insight on the kind of photocatalysts and combinations that have advanced the field and that have mostly been explored. It can be clearly seen that metal oxides, such as BiVO$_4$ or WO$_3$, are commonly used as OEP. Z-Scheme constructed with oxynitrides or oxysulfides (as HEP) in combination with BiVO$_4$ or WO$_3$ (as OEP) achieved lower AQY compared to implementations composed of only metal oxides. The poor selectivity of surface chemical reaction in presence of reversible redox mediators seems to be a major challenge. Moreover, oxynitrides and oxysulfide photocatalysts are not stable enough during water splitting reactions as they are susceptible towards self-oxidation by photo-excited holes. Recently, Takata et al. reported AQY higher than 95% at wavelength 350–360 nm for SrTiO$_3$:Al in one-step overall water splitting, achieving an STH 0.65%.[11] However, the theoretical maximum STH obtainable from SrTiO$_3$:Al is less than 1.4% (even if AQY reaches 100% at all wavelengths below 380 nm), limited by the short absorption edge of the photocatalyst. Thus, the development of durable oxynitride and oxysulfide materials (as both HEP and OEP) that can utilize photons at wavelength up to 700 nm is essential.

Reported demonstrations of Z-schemes have been mostly evaluated in type 2* reactors, where two photocatalysts are combined in a single compartment causing the mixing of product gases. Qi et al. achieved an STH efficiency of 0.5% using a soluble redox mediator[35] for the combination TaON and BiVO$_4$ (bandgap energy 2.4 eV) where the maximum theoretical efficiency of the aforementioned materials combination is 4.7%. There are improvements needed in the charge separation and transport properties to achieve efficiencies closer to this theoretical value. Water splitting efficiency of oxynitride and oxysulfide based systems for HEPs are still limited because these materials were utilized with relatively wide bandgap semiconductors (WO$_3$, BiVO$_4$ or TiO$_2$) in the presence of an IO$_3^-$/I$^-$ redox mediator, which undergoes rapid backward reaction and involves multi-electron transfer for the redox reaction. Photocatalysts with bandgap energies $\leq$ 2.0 eV were rarely employed in Z-scheme overall water splitting reactions. Though there are some photocatalysts, such as La$_5$Ti$_2$Cu$_{0.9}$Ag$_{0.1}$O$_5$S$_7$, BaTaO$_2$N, LaTiO$_2$N, available with bandgap energies around 1.9 eV, they have not yet been investigated in detail in a Z-scheme with an appropriate redox mediator. One of the main obstacles of this research field is the limited choices for OEP as an alternative to BiVO$_4$ and Bi$_4$NbO$_8$Cl and with a bandgap energy closer to and even smaller than 1.5 eV. The recently discovered Y$_2$Ti$_2$O$_5$S$_2$ (1.9 eV) or LaNbON$_2$ (ref. 67) (1.65 eV) could be interesting OEPs in a Z-scheme. Schematic band diagrams of various semiconductor photocatalysts are presented in Fig. 8.

According to the modeling predictions of the maximum theoretical STH efficiency in tandem and side-by-side configuration for reactor types 2 and 3 (type 3 only possible in tandem configuration), it is most beneficial to combine 0.6–1.8 eV

bandgap energies of the bottom photocatalyst with 1.55–2.4 eV bandgap energies of the top photocatalyst for a mediator redox range of 0.2 to 1.0 V (*vs.* SHE). A smaller redox potential of the mediator favors larger photocatalyst bandgaps but at the expense of reduced potential in the overall efficiency. Bi_2S_3, $LaNbON_2$, $Y_2Ti_2O_5S_2$ and $LaTiO_2N$ are few possible choices for OEP in the bandgap range of 0.7–1.9 eV. A number of choices for HEPs are available, given the more flexible range of 1.5–2.4 eV (for *e.g.* $CuFeO_2$, $CuBi_2O_4$, $CaFe_2O_4$, Ta_3N_5, $TaON$, $BaTaO_2N$, $CuInS_2$, $AgIn_5S_8$, $La_5Ti_2CuS_5O_7$), that could be combined with Bi_2S_3, $LaNbON_2$, $Y_2Ti_2O_5S_2$ or $LaTiO_2N$. The equilibrium potential of the redox mediators may vary from 0.2–1.2 V (*vs.* SHE). The potentials of typical redox mediators are also indicated in Fig. 8.

5. Conclusion and outlook

Photocatalytic water splitting has been identified as a promising and economically competitive approach for solar hydrogen generation.[3,7,68] However, the implementation of photocatalytic approaches into practical and scalable solar hydrogen processing systems is yet to be designed and demonstrated. Most of the practically demonstrated Z-scheme reactors are laboratory-scale demonstrations that do not allow for product separation as they lead to co-evolution of hydrogen and oxygen inside the reactor. Furthermore, it is not clear and quantified how conceptual as well as practical designs of photocatalytic reactors are affecting the overall water splitting efficiency and what are their limiting efficiencies. Key uncertainties and challenges remain in the conceptual and practical design, implementation and optimization of functional and scalable reactors, and the understanding if and to what extend the conceptual reactor design affects the best choice of photocatalyst, co-catalysts, mediators, and membranes.

Here, we highlight the relation between conceptual reactor design, choice of materials, and theoretical efficiencies, with the aim to guide the material science and development for efficient and practical photocatalystic water splitting. We review and systematically group and compare possible conceptual designs for photocatalytic particle-suspension reactors, quantify their theoretical limiting efficiencies, and relate these calculations to the requirements on photocatalyst, mediator species and membranes. We then compare the theoretical predictions to the trends in material synthesis and laboratory demonstrations in order to provide broader recommendations on material research. Two of the three general reactor concepts introduced in our study allow for inherent product separation through the use of two spatially-separated photocatalysts and a liquid redox mediator acting as shuttle between them. These two photocatalyst suspension approaches (termed type 2 and type 3) allow for more flexibility in choices of materials for photocatalyst, cocatalyst, electrolyte, mediator, and membrane. This flexibility is pushed further in type 3, where (at the expense of the added overpotentials and the requirement for a more tailored membrane) the two photocatalysts (HEP and OEP) can operate with different redox mediators.

A summary and overview of the discussed photocatalytic particle suspension reactors, their maximum theoretical STH efficiencies, and best practical demonstrations are given in Fig. 9. Laboratory-scale demonstrations of Z-scheme are usually performed in a single compartment type 2* reactor causing mixing of products. The highest STH ever reported using two photocatalysts with a soluble redox mediator is 0.5%,[35] several times lower than the corresponding theoretical value of 4.91%. Whereas, type 2 reactor can achieve maximum theoretical efficiency of 32.33% (at HEP/OEP bandgap energies of 1.65/0.8 eV and a redox mediator with a potential of 1.0 V *vs.* SHE). This indicates that careful consideration of photocatalyst material and redox mediators are indispensable to realize maximum solar energy conversion.

In our study, recent progress in overall water splitting research has been also summarized in terms of novel photocatalysts development and their gas evolution efficiency under visible light. Till date, a large number of photocatalysts have been developed and remarkable progress has been achieved in this research field. The record STH efficiency of 1.0% has been achieved in Z-scheme overall water splitting at ambient pressure using photocatalyst sheets (*i.e.* immobilized photocatalyst particles) composed of metal oxides utilizing visible light up to ~500 nm wavelength. In particulate suspension-based Z-schemes, a record STH efficiency of 0.5% was achieved for the combination $(Pt/ZrO_2/TaON)–[Fe(CN)_6]^{3-/4-}–(AuNPs/CoO_x/BiVO_4)$. This system utilized visible light up to ~520 nm. Some other reported Z-schemes composed of non-oxide photocatalysts (for *e.g.* HEP: $La_5Ti_2Cu_{0.9}Ag_{0.1}S_5O_7$:Ga, $LaMg_{1/3}Ta_{2/3}O_2N$, $BaTaO_2N$; OEP: $LaTiO_2N$)[62–64] absorbing visible light ~600 nm but still STH efficiencies achieved were several folds lower than 1.0%,[64] primarily because of the lower AQY compared to what is typically achieved when using metal oxide (bandgap energy $\geq$ 2.4 eV) photocatalysts. The number of available HEPs absorbing visible light at wavelength longer than 700 nm is limited and has yet to be investigated in an overall water splitting reaction.[65,69,70]

For commercial and economically viable solar hydrogen production, STH efficiencies should reach more than just 1–2% at ambient pressure. Thus, it is necessary not only to replace wide band gap metal oxides with the typically narrower band gap (oxy)nitride and (oxy)sulfide photocatalysts but also to prevent the backward reactions at elevated pressure. To achieve comparable AQY for non-oxide photocatalysts and metal oxide semiconductors, emphasis should be put on controlling the particle size and morphology by refining materials synthesis methods which can reduce defect densities (commonly known to act as charge recombination center), by optimizing cocatalyst and the selective deposition of dual cocatalysts (with different functionality to extract e^- and h^+ from the bulk) to facilitate transport of excited charge carriers to the reaction sites, by coating layers onto cocatalysts, photocatalysts and even exposed Au surface for sheet systems to inhibit backward reactions, and by bandgap engineering through the formation of solid solutions.

A broad range of reversible, non-absorbing redox mediators should be available so as to cover the large range of redox

potentials (ideally from 0.2 to 1.2 V *vs.* SHE) and, therefore, to enable a large flexibility in the implementation of various photocatalysts. Consequently, a wider range of redox mediators should be explored, implemented, and investigated with respect to their activity, reversibility, and selectivity for various photocatalysts and – potentially – efforts for the development of dedicated and tailored cocatalysts need to be intensified.

Another important factor toward practical implementation of reactor design is the pH dependence of the photocatalyst (Table 1 and Fig. 8) crucial for the long-term stability of overall water splitting system. Most of the efficient and earth-abundant OEPs are not stable in acidic condition, and *vice versa*; whereas, most of the earth-abundant HEPs are not stable in base.[71,72] Thus, it is advantageous if two compartment reactors can be operated for respective gas evolution reactions which can be operated at different (acidic/basic) pH suitable for the corresponding materials. The bipolar membrane (BPM) offers such flexibility by separating the electrolytes of the two compartments and maintaining a high pH gradient. A possible new reactor could integrate the BPM as a version of reactor type 3 so as to operate the compartments at acidic and basic pH.

Theoretical modeling predicted the possibility to achieve maximum STH efficiencies in the range of ∼30% STH (for ideal case) for all three types of reactor (Fig. 9), indicating the interesting and large potential of these approaches. Additionally, the theoretical modeling provides a better understanding of the best possible choices of photocatalysts and mediators to achieve these maximum efficiencies and the most critical obstacles to improve energy conversion efficiency of the reactors. The comparison between the material combinations that lead to the best theoretical efficiencies and the practical demonstrations highlight the areas that should be intensified for materials research and development. Future demonstrations and research should focus onto type 2 and type 3 reactors to perform Z-scheme overall water splitting reaction as they allow for inherent product separation and enable larger flexibility in combination of materials. Generally, lower bandgap OEP and HEP are desired, and the importance of characterization and optimization of mediator redox reactions at these OEPs and HEPs becomes apparent. Furthermore, a conscious choice of the redox mediator potential allows for a larger choice of OEP and HEP, generally requiring larger bandgap OEP and HEP with less matched mediator potentials.

Bi_2S_3, $LaNbON_2$, $Y_2Ti_2O_5S_2$ and $LaTiO_2N$ are potentially advantageous photocatalysts to be used for O_2 evolution compared to the more widely known $BiVO_4$ and Bi_4NbO_8Cl, in combination with HEPs available in the bandgap energy range 1.5–2.4 eV. It is also essential to develop active and selective OEPs with bandgap energies even below 1.5 eV. A number of candidates for HEPs are available, such as $CuFeO_2$, $CuBi_2O_4$, $CaFe_2O_4$, Ta_3N_5, TaON, $BaTaO_2N$, $CuInS_2$, $AgIn_5S_8$, $La_5Ti_2CuS_5$-O_7. The careful choice of the top-bottom arrangement of suspension reactors (HEP on top or OEP on top) further allows for more flexibility in choosing photocatalysts, *i.e.* the photocatalyst chosen in the top compartment is required to have a larger bandgap.

By reviewing the material status of photocatalytic water splitting and combining this review with theoretical maximum efficiency analysis, we provide a general understanding of the state-of-the art in the field and are able to identify conceptually interesting reactor design strategies and needs for materials development in order to reach the potential of photocatalytic suspension reactors, eventually leading to practical, scalable and durable solar hydrogen production *via* two-step photocatalytic overall water splitting.

Data availability

The datasets generated and/or analysed during the current study are avaialble from the corresponding author on reasonable request.

Author contributions

S. N. reviewed the theory and materials. S. S. developed and performed the simulations on conceptual reactor designs. S. N., S. S. and S. H. wrote the paper. S. H. directed the research. S. N. and S. S. are equally contributing authors.

Conflicts of interest

There are no conflicts to declare.

Acknowledgements

References

1 M. G. Walter, E. L. Warren, J. R. McKone, S. W. Boettcher, Q. Mi, E. A. Santori and N. S. Lewis, Solar Water Splitting Cells, *Chem. Rev.*, 2010, **110**, 6446–6473.

2 A. Kudo and Y. Miseki, Heterogeneous photocatalyst materials for water splitting, *Chem. Soc. Rev.*, 2009, **38**, 253–278.

3 T. Hisatomi, J. Kubota and K. Domen, Recent advances in semiconductors for photocatalytic and photoelectrochemical water splitting, *Chem. Soc. Rev.*, 2014, **43**, 7520–7535.

4 K. Domen, S. Naito, M. Soma, T. Onishi and K. Tamaru, Photocatalytic decomposition of water vapour on an NiO–$SrTiO_3$ catalyst, *J. Chem. Soc., Chem. Commun.*, 1980, 543–544.

5 Y. Matsumoto, M. Obata and J. Hombo, Photocatalytic Reduction of Carbon-Dioxide on P-Type $CaFe_2O_4$ Powder, *J. Phys. Chem.*, 1994, **98**, 2950–2951.

6 Q. Liu, Z.-X. Low, L. Li, A. Razmjou, K. Wang, J. Yao and H. Wang, ZIF-8/Zn$_2$GeO$_4$ nanorods with an enhanced CO$_2$ adsorption property in an aqueous medium for photocatalytic synthesis of liquid fuel, *J. Mater. Chem. A*, 2013, **1**, 11563.

7 T. Takata and K. Domen, Particulate Photocatalysts for Water Splitting: Recent Advances and Future Prospects, *ACS Energy Lett.*, 2019, **4**, 542–549.

8 S. Keene, R. Bala Chandran and S. Ardo, Calculations of theoretical efficiencies for electrochemically-mediated tandem solar water splitting as a function of bandgap energies and redox shuttle potential, *Energy Environ. Sci.*, 2019, **12**, 261–272.

9 Z. Chen, T. F. Jaramillo, T. G. Deutsch, A. Kleiman-Shwarsctein, A. J. Forman, N. Gaillard, R. Garland, K. Takanabe, C. Heske, M. Sunkara, E. W. McFarland, K. Domen, E. L. Miller, J. A. Turner and H. N. Dinh, Accelerating materials development for photoelectrochemical hydrogen production: standards for methods, definitions, and reporting protocols, *J. Mater. Res.*, 2011, **25**, 3–16.

10 H. Kato, K. Asakura and A. Kudo, Highly Efficient Water Splitting into H$_2$ and O$_2$ over Lanthanum-Doped NaTaO$_3$ Photocatalysts with High Crystallinity and Surface Nanostructure, *J. Am. Chem. Soc.*, 2003, **125**, 3082–3089.

11 T. Takata, J. Jiang, Y. Sakata, M. Nakabayashi, N. Shibata, V. Nandal, K. Seki, T. Hisatomi and K. Domen, Photocatalytic water splitting with a quantum efficiency of almost unity, *Nature*, 2020, **581**, 411–414.

12 F. E. Osterloh, Inorganic Materials as Catalysts for Photochemical Splitting of Water, *Chem. Mater.*, 2008, **20**, 35–54.

13 Y. Inoue, Photocatalytic water splitting by RuO$_2$-loaded metal oxides and nitrides with d0- and d10-related electronic configurations, *Energy Environ. Sci.*, 2009, **2**, 364.

14 G. Liu, K. Du, S. Haussener and K. Wang, Charge Transport in Two-Photon Semiconducting Structures for Solar Fuels, *ChemSusChem*, 2016, **9**, 2878–2904.

15 K. Maeda, Z-Scheme Water Splitting Using Two Different Semiconductor Photocatalysts, *ACS Catal.*, 2013, **3**, 1486–1503.

16 K. T. Fountaine, H. J. Lewerenz and H. A. Atwater, Efficiency limits for photoelectrochemical water-splitting, *Nat. Commun.*, 2016, **7**, 13706.

17 Y. Wang, H. Suzuki, J. Xie, O. Tomita, D. J. Martin, M. Higashi, D. Kong, R. Abe and J. Tang, Mimicking Natural Photosynthesis: Solar to Renewable H$_2$ Fuel Synthesis by Z-Scheme Water Splitting Systems, *Chem. Rev.*, 2018, **118**, 5201–5241.

18 Q. Wang and K. Domen, Particulate Photocatalysts for Light-Driven Water Splitting: Mechanisms, Challenges, and Design Strategies, *Chem. Rev.*, 2020, **120**, 919–985.

19 J. Yang, D. Wang, H. Han and C. Li, Roles of Cocatalysts in Photocatalysis and Photoelectrocatalysis, *Acc. Chem. Res.*, 2013, **46**, 1900–1909.

20 R. Bala Chandran, S. Breen, Y. Shao, S. Ardo and A. Z. Weber, Evaluating particle-suspension reactor designs for Z-scheme solar water splitting *via* transport and kinetic modeling, *Energy Environ. Sci.*, 2018, **11**, 115–135.

21 S. Nandy, T. Hisatomi, G. Ma, T. Minegishi, M. Katayama and K. Domen, Enhancement of the H$_2$ evolution activity of La$_5$Ti$_2$Cu(S$_{1-x}$Se$_x$)$_5$O$_7$ photocatalysts by coloading Pt and NiS cocatalysts, *J. Mater. Chem. A*, 2017, **5**, 6106–6112.

22 D. Bae, B. Seger, P. C. K. Vesborg, O. Hansen and I. Chorkendorff, Strategies for stable water splitting *via* protected photoelectrodes, *Chem. Soc. Rev.*, 2017, **46**, 1933–1954.

23 C. C. L. McCrory, S. Jung, I. M. Ferrer, S. M. Chatman, J. C. Peters and T. F. Jaramillo, Benchmarking Hydrogen Evolving Reaction and Oxygen Evolving Reaction Electrocatalysts for Solar Water Splitting Devices, *J. Am. Chem. Soc.*, 2015, **137**, 4347–4357.

24 K. Maeda and K. Domen, New Non-Oxide Photocatalysts Designed for Overall Water Splitting under Visible Light, *J. Phys. Chem. C*, 2007, **111**, 7851–7861.

25 K. Maeda, K. Teramura, D. Lu, T. Takata, N. Saito, Y. Inoue and K. Domen, Photocatalyst releasing hydrogen from water, *Nature*, 2006, **440**, 295.

26 J. Sato, N. Saito, Y. Yamada, K. Maeda, T. Takata, J. N. Kondo, M. Hara, H. Kobayashi, K. Domen and Y. Inoue, RuO$_2$-Loaded β-Ge$_3$N$_4$ as a Non-Oxide Photocatalyst for Overall Water Splitting, *J. Am. Chem. Soc.*, 2005, **127**, 4150–4151.

27 Z. Wang, Y. Inoue, T. Hisatomi, R. Ishikawa, Q. Wang, T. Takata, S. Chen, N. Shibata, Y. Ikuhara and K. Domen, Overall water splitting by Ta$_3$N$_5$ nanorod single crystals grown on the edges of KTaO$_3$ particles, *Nat. Catal.*, 2018, **1**, 756–763.

28 K. Sayama, R. Yoshida, H. Kusama, K. Okabe, Y. Abe and H. Arakawa, Photocatalytic decomposition of water into H$_2$ and O$_2$ by a two-step photoexcitation reaction using a WO$_3$ suspension catalyst and an Fe^{3+}/Fe^{2+} redox system, *Chem. Phys. Lett.*, 1997, **277**, 387–391.

29 M. Higashi, R. Abe, K. Teramura, T. Takata, B. Ohtani and K. Domen, Two step water splitting into H$_2$ and O$_2$ under visible light by ATaO$_2$N (A = Ca, Sr, Ba) and WO$_3$ with IO$_3^-$/I$^-$ shuttle redox mediator, *Chem. Phys. Lett.*, 2008, **452**, 120–123.

30 R. Abe, K. Sayama and H. Sugihara, Development of New Photocatalytic Water Splitting into H$_2$ and O$_2$ using Two Different Semiconductor Photocatalysts and a Shuttle Redox Mediator IO$_3^-$/I$^-$, *J. Phys. Chem. B*, 2005, **109**, 16052–16061.

31 Y. Goto, T. Hisatomi, Q. Wang, T. Higashi, K. Ishikiriyama, T. Maeda, Y. Sakata, S. Okunaka, H. Tokudome, M. Katayama, S. Akiyama, H. Nishiyama, Y. Inoue, T. Takewaki, T. Setoyama, T. Minegishi, T. Takata, T. Yamada and K. Domen, A Particulate Photocatalyst Water-Splitting Panel for Large-Scale Solar Hydrogen Generation, *Joule*, 2018, **2**, 509–520.

32 Q. Wang, M. Nakabayashi, T. Hisatomi, S. Sun, S. Akiyama, Z. Wang, Z. Pan, X. Xiao, T. Watanabe, T. Yamada, N. Shibata, T. Takata and K. Domen, Oxysulfide photocatalyst for visible-light-driven overall water splitting, *Nat. Mater.*, 2019, **18**, 827–832.

33 S. Hu, C. Xiang, S. Haussener, A. D. Berger and N. S. Lewis, An analysis of the optimal band gaps of light absorbers in integrated tandem photoelectrochemical water-splitting systems, *Energy Environ. Sci.*, 2013, **6**, 2984.

34 T. Luo, S. Abdu and M. Wessling, Selectivity of ion exchange membranes: a review, *J. Membr. Sci.*, 2018, **555**, 429–454.

35 Y. Qi, Y. Zhao, Y. Gao, D. Li, Z. Li, F. Zhang and C. Li, Redox-Based Visible-Light-Driven Z-Scheme Overall Water Splitting with Apparent Quantum Efficiency Exceeding 10%, *Joule*, 2018, **2**, 2393–2402.

36 R. Abe, K. Sayama and H. Arakawa, Significant influence of solvent on hydrogen production from aqueous I^{3-}/I^- redox solution using dye-sensitized Pt/TiO_2 photocatalyst under visible light irradiation, *Chem. Phys. Lett.*, 2003, **379**, 230–235.

37 Z. B. Yu, Y. P. Xie, G. Liu, G. Q. Lu, X. L. Ma and H.-M. Cheng, Self-assembled CdS/Au/ZnO heterostructure induced by surface polar charges for efficient photocatalytic hydrogen evolution, *J. Mater. Chem. A*, 2013, **1**, 2773.

38 K. Fujihara, T. Ohno and M. Matsumura, Splitting of water by electrochemical combination of two photocatalytic reactions on TiO_2 particles, *J. Chem. Soc., Faraday Trans.*, 1998, **94**, 3705–3709.

39 E. E. M. Cating, C. W. Pinion, J. D. Christesen, C. A. Christie, E. M. Grumstrup, J. F. Cahoon and J. M. Papanikolas, Probing Intrawire, Interwire, and Diameter-Dependent Variations in Silicon Nanowire Surface Trap Density with Pump–Probe Microscopy, *Nano Lett.*, 2017, **17**, 5956–5961.

40 D. M. Fabian, S. Hu, N. Singh, F. A. Houle, T. Hisatomi, K. Domen, F. E. Osterloh and S. Ardo, Particle suspension reactors and materials for solar-driven water splitting, *Energy Environ. Sci.*, 2015, **8**, 2825–2850.

41 M. D. L. M. Ballari, R. Brandi, O. Alfano and A. Cassano, Mass transfer limitations in photocatalytic reactors employing titanium dioxide suspensions, *Chem. Eng. J.*, 2008, **136**, 50–65.

42 K. Sayama, K. Mukasa, R. Abe, Y. Abe and H. Arakawa, Stoichiometric water splitting into H_2 and O_2 using a mixture of two different photocatalysts and an IO_3^-/I^- shuttle redox mediator under visible light irradiation, *Chem. Commun.*, 2001, 2416–2417.

43 R. Niishiro, S. Tanaka and A. Kudo, Hydrothermal-synthesized $SrTiO_3$ photocatalyst codoped with rhodium and antimony with visible-light response for sacrificial H_2 and O_2 evolution and application to overall water splitting, *Appl. Catal., B*, 2014, **150–151**, 187–196.

44 H. Kato, M. Hori, R. Konta, Y. Shimodaira and A. Kudo, Construction of Z-scheme Type Heterogeneous Photocatalysis Systems for Water Splitting into H_2 and O_2 under Visible Light Irradiation, *Chem. Lett.*, 2004, **33**, 1348–1349.

45 H. Kato, Y. Sasaki, N. Shirakura and A. Kudo, Synthesis of highly active rhodium-doped $SrTiO_3$ powders in Z-scheme systems for visible-light-driven photocatalytic overall water splitting, *J. Mater. Chem. A*, 2013, **1**, 12327–12333.

46 Y. Sasaki, H. Kato and A. Kudo, $[Co(bpy)_3]^{3+/2+}$ and $[Co(phen)_3]^{3+/2+}$ Electron Mediators for Overall Water Splitting under Sunlight Irradiation Using Z-Scheme Photocatalyst System, *J. Am. Chem. Soc.*, 2013, **135**, 5441–5449.

47 Y. Sasaki, A. Iwase, H. Kato and A. Kudo, The effect of co-catalyst for Z-scheme photocatalysis systems with an Fe^{3+}/Fe^{2+} electron mediator on overall water splitting under visible light irradiation, *J. Catal.*, 2008, **259**, 133–137.

48 A. Nakada, A. Saeki, M. Higashi, H. Kageyama and R. Abe, Two-step synthesis of Sillén–Aurivillius type oxychlorides to enhance their photocatalytic activity for visible-light-induced water splitting, *J. Mater. Chem. A*, 2018, **6**, 10909–10917.

49 K. Ogawa, A. Nakada, H. Suzuki, O. Tomita, M. Higashi, A. Saeki, H. Kageyama and R. Abe, Flux Synthesis of Layered Oxyhalide Bi_4NbO_8Cl Photocatalyst for Efficient Z-Scheme Water Splitting Under Visible Light, *ACS Appl. Mater. Interfaces*, 2019, **11**, 5642–5650.

50 R. Abe, T. Takata, H. Sugihara and K. Domen, Photocatalytic overall water splitting under visible light by TaON and WO_3 with an IO_3^-/I^- shuttle redox mediator, *Chem. Commun.*, 2005, 3829–3831.

51 K. Maeda, M. Higashi, D. Lu, R. Abe and K. Domen, Efficient Nonsacrificial Water Splitting through Two-Step Photoexcitation by Visible Light using a Modified Oxynitride as a Hydrogen Evolution Photocatalyst, *J. Am. Chem. Soc.*, 2010, **132**, 5858–5868.

52 K. Maeda, R. Abe and K. Domen, Role and Function of Ruthenium Species as Promoters with TaON-Based Photocatalysts for Oxygen Evolution in Two-Step Water Splitting under Visible Light, *J. Phys. Chem. C*, 2011, **115**, 3057–3064.

53 M. Higashi, R. Abe, T. Takata and K. Domen, Photocatalytic Overall Water Splitting under Visible Light Using $ATaO_2N$ (A = Ca, Sr, Ba) and WO_3 in a IO_3^-/I^- Shuttle Redox Mediated System, *Chem. Mater.*, 2009, **21**, 1543–1549.

54 K. Maeda, D. Lu and K. Domen, Solar-Driven Z-scheme Water Splitting Using Modified $BaZrO_3$–$BaTaO_2N$ Solid Solutions as Photocatalysts, *ACS Catal.*, 2013, **3**, 1026–1033.

55 S. Chen, Y. Qi, T. Hisatomi, Q. Ding, T. Asai, Z. Li, S. S. K. Ma, F. Zhang, K. Domen and C. Li, Efficient Visible-Light-Driven Z-Scheme Overall Water Splitting Using a $MgTa_2O_{6-x}N_y/TaON$ Heterostructure Photocatalyst for H_2 Evolution, *Angew. Chem., Int. Ed.*, 2015, **54**, 8498–8501.

56 W. Zhao, K. Maeda, F. Zhang, T. Hisatomi and K. Domen, Effect of post-treatments on the photocatalytic activity of $Sm_2Ti_2S_2O_5$ for the hydrogen evolution reaction, *Phys. Chem. Chem. Phys.*, 2014, **16**, 12051–12056.

57 T. Kato, Y. Hakari, S. Ikeda, Q. Jia, A. Iwase and A. Kudo, Utilization of Metal Sulfide Material of $(CuGa)_{1-x}Zn_{2x}S_2$ Solid Solution with Visible Light Response in Photocatalytic and Photoelectrochemical Solar Water Splitting Systems, *J. Phys. Chem. Lett.*, 2015, **6**, 1042–1047.

58 Z. Song, T. Hisatomi, S. Chen, Q. Wang, G. Ma, S. Li, X. Zhu, S. Sun and K. Domen, Visible-Light-Driven Photocatalytic Z-Scheme Overall Water Splitting in $La_5Ti_2AgS_5O_7$-based Powder-Suspension System, *ChemSusChem*, 2019, **12**, 1906–1910.

59 A. Iwase, Y. H. Ng, Y. Ishiguro, A. Kudo and R. Amal, Reduced graphene oxide as a solid-state electron mediator in Z-scheme photocatalytic water splitting under visible light, *J. Am. Chem. Soc.*, 2011, **133**, 11054–11057.

60 Q. Wang, T. Hisatomi, Q. Jia, H. Tokudome, M. Zhong, C. Wang, Z. Pan, T. Takata, M. Nakabayashi, N. Shibata, Y. Li, I. D. Sharp, A. Kudo, T. Yamada and K. Domen, Scalable water splitting on particulate photocatalyst sheets with a solar-to-hydrogen energy conversion efficiency exceeding 1%, *Nat. Mater.*, 2016, **15**, 611.

61 Q. Wang, T. Hisatomi, Y. Suzuki, Z. Pan, J. Seo, M. Katayama, T. Minegishi, H. Nishiyama, T. Takata, K. Seki, A. Kudo, T. Yamada and K. Domen, Particulate Photocatalyst Sheets Based on Carbon Conductor Layer for Efficient Z-Scheme Pure-Water Splitting at Ambient Pressure, *J. Am. Chem. Soc.*, 2017, **139**, 1675–1683.

62 Z. Pan, T. Hisatomi, Q. Wang, M. Nakabayashi, N. Shibata, C. Pan, T. Takata and K. Domen, Application of $LaMg_{1/3}Ta_{2/3}O_2N$ as a hydrogen evolution photocatalyst of a photocatalyst sheet for Z-scheme water splitting, *Appl. Catal., A*, 2016, **521**, 26–33.

63 S. Sun, T. Hisatomi, Q. Wang, S. Chen, G. Ma, J. Liu, S. Nandy, T. Minegishi, M. Katayama and K. Domen, Efficient Redox-Mediator-Free Z-Scheme Water Splitting Employing Oxysulfide Photocatalysts under Visible Light, *ACS Catal.*, 2018, **8**, 1690–1696.

64 T. Hisatomi, T. Yamamoto, Q. Wang, T. Nakanishi, T. Higashi, M. Katayama, T. Minegishi and K. Domen, Particulate photocatalyst sheets based on non-oxide semiconductor materials for water splitting under visible light irradiation, *Catal. Sci. Technol.*, 2018, **8**, 3918–3925.

65 S. Nandy, Y. Goto, T. Hisatomi, Y. Moriya, T. Minegishi, M. Katayama and K. Domen, Synthesis and Photocatalytic Activity of $La_5Ti_2Cu(S_{1-x}Se_x)_5O_7$ Solid Solutions for H_2 Production under Visible Light Irradiation, *ChemPhotoChem*, 2017, **1**, 265–272.

66 B. Dong, J. Cui, Y. Gao, Y. Qi, F. Zhang and C. Li, Heterostructure of 1D Ta_3N_5 Nanorod/$BaTaO_2$ N Nanoparticle Fabricated by a One-Step Ammonia Thermal Route for Remarkably Promoted Solar Hydrogen Production, *Adv. Mater.*, 2019, **31**, e1808185.

67 X. Wang, T. Hisatomi, J. Liang, Z. Wang, Y. Xiang, Y. Zhao, X. Dai, T. Takata and K. Domen, Facet engineering of $LaNbON_2$ transformed from $LaKNaNbO_5$ for enhanced photocatalytic O_2 evolution, *J. Mater. Chem. A*, 2020, **8**, 11743–11751.

68 B. A. Pinaud, J. D. Benck, L. C. Seitz, A. J. Forman, Z. Chen, T. G. Deutsch, B. D. James, K. N. Baum, G. N. Baum, S. Ardo, H. Wang, E. Miller and T. F. Jaramillo, Technical and economic feasibility of centralized facilities for solar hydrogen production *via* photocatalysis and photoelectrochemistry, *Energy Environ. Sci.*, 2013, **6**, 1983–2002.

69 S. Chen, J. J. M. Vequizo, T. Hisatomi, M. Nakabayashi, L. Lin, Z. Wang, A. Yamakata, N. Shibata, T. Takata, T. Yamada and K. Domen, Efficient photocatalytic hydrogen evolution on single-crystalline metal selenide particles with suitable cocatalysts, *Chem. Sci.*, 2020, **19**, 631.

70 S. Nandy, T. Hisatomi, S. Sun, M. Katayama, T. Minegishi and K. Domen, Effects of Se Incorporation in $La_5Ti_2CuS_5O_7$ by Annealing on Physical Properties and Photocatalytic H_2 Evolution Activity, *ACS Appl. Mater. Interfaces*, 2019, **11**, 5595–5601.

71 J. Luo, D. A. Vermaas, D. Bi, A. Hagfeldt, W. A. Smith and M. Grätzel, Bipolar Membrane-Assisted Solar Water Splitting in Optimal pH, *Adv. Energy Mater.*, 2016, **6**, 1600100.

72 D. A. Vermaas, M. Sassenburg and W. A. Smith, Photo-assisted water splitting with bipolar membrane induced pH gradients for practical solar fuel devices, *J. Mater. Chem. A*, 2015, **3**, 19556–19562.